QATAR UNIVERSITY

COLLEGE OF ARTS AND SCIENCES

SINGLE STEP ELECTRODEPOSITION OF CZTS ABSORBER LAYER FOR SOLAR CELLS APPLICATION

BY

Latifa Khaled Al-Romaihi

A Thesis Submitted to the Faculty of

the College of Arts and Sciences

in Partial Fulfillment

of the Requirements

for the Degree of

Masters of Science

in

Material Science and Technology

June 2018

COMMITTEE PAGE

The members of the Committee approve the Thesis of Latifa Khaled AlRomaihi defended on 20/05/2018.

_____

Prof. Talal Altahtamouni
Thesis/Dissertation Supervisor

_____

Prof. Aboubakr Ali
Co-supervisor

_____

Dr. Zubair Ahmad
Committee Member

_____

Dr. Said Mansour
Committee Member

Approved:

_____

Rashid Al-Kuwari, Dean, College of College of Arts and Sciences

ABSTRACT

ALROMAIHI, LATIFA, KHALED., Masters : June : [2018:], Material Science and Technology

Title: Single Step Electrodeposition of CZTS Absorber Layer for Solar Cells Application

Supervisor of Thesis: Prof. Talal, M. Altahtamouni.

Nowadays, one of the most critical issues in photovoltaic (PV) industry is the fabrication of an efficient and low cost solar cells. The solar energy have to be more efficient and cost effective than other electricity sources in order to be a major source of electricity. Different types of photovoltaic materials have been developed over the past century and the latest technology is based on thin film solar cells. Copper indium gallium selenide (CIGS) thin film based solar cells have achieved more than 20% power conversion efficiency. However, these materials are toxic, rare and expensive. Copper zinc tin sulfide (CZTS) is a very promising material and a good alternative for CIGS thin film. CZTS materials are cheap, non-toxic and abundant. Also, It has an ideal band gap of 1.5 eV and a high absorption coefficient.

Single step electrodeposition technique was used to deposit CZTS thin film on fluorine doped tin oxide (FTO) coated glass substrate. In order to identify the suitable deposition potential, a set of CZTS thin films were deposited at different potentials. The used potentials were -1.10 V, -1.20 V, -1.25 V, -1.30 V, and -1.35 V (vs. Ag/AgCl). XRD and Raman analysis were used to confirm the presence of CZTS kesterite phase. There was a dependence for the intensity and FWHM of the (112) planes peaks which affect the crystallite size. The sample deposited at -1.35 V had the highest crystal size and the best

crystalline quality. The EDS and XPS measurements were performed and the best stoichiometry was achieved in the sample deposited at -1.35 V.

The influence of sulfur amount in the sulfurization process on the CZTS thin films was also investigated. So, a set of CZTS films was electrodiposited using -1.35 V and sulfurized using 5 mg, 15 mg, 25 mg, 35 mg, and 50 mg of sulfur powder. The best CZTS thin film stoichiometry and crystalline quality was achieved using 35 mg sulfur according to XRD, Raman and EDS analyses. Uv-visible and Photoluminescence (PL) measurements were used to study the optical properties of the electrodeposited films. The sample electrodeposited at -1.35 V using 35 mg sulfur exhibited a 1.50 eV optical band gap and 10^4 cm^{-1} absorption coefficient. These results confirm the suitability of these films to be utilized as absorber layers in thin film solar cell structures.

DEDICATION

This thesis is dedicated to my parents who taught me to trust in Allah, and encouraged me to believe in myself. Also to my husband who gave me his full support to achieve my goals.

ACKNOWLEDGMENTS

I would like to express my thanks and gratitude to my supervisor Prof. Talal Altahtamouni and my co-supervisor Prof. Aboubakr Ali for their support, encouragement and guidance during my thesis work. I am grateful to other members in my thesis committee, Dr. Zubair Ahmad and Dr. Said Mansour, I appreciate their support and time. I also would like to thank the faculty at the Materials Science and Technology Program, Dr. Ahmed Elzatahry and Dr. Khaled Youssef.

I would like to thank my colleagues and Lab technicians for their assistance and useful discussions. Special thanks goes to the staff at the Central Laboratory Unit (CLU) at the College of Arts and Sciences and the Center for Advanced Materials (CAM) for their support during my research work. In addition, I would like to thank Dr. Said Mansour and his team from HBKU for providing characterization to some of my samples.

I appreciate and acknowledge the financial support by Qatar University student grant number QUST-1-CAS-2018-49

TABLE OF CONTENTS

DEDICATION v
ACKNOWLEDGMENTS vi
LIST OF TABLES ix
LIST OF FIGURES x
CHAPTER 1: INTRODUCTION 1
1. Solar energy 1
2. Photovoltaic (PV) technology and material 1
3. Thin film solar cell 2
4. CZTS thin film solar cell 2
4.1. CZTS material 2
4.2. Structure of CZTS absorber layer for solar cells 6
4.3. Working principle of CZTS absorber layer for solar cells 8
CHAPTER 2: LITERATURE REVIEW 10
1. Solar cells generations 10
2. CZTS Thin film 12
3. Electrodeposition technique: 13
3.1. Stacked elemental layer (SEL) or binary alloys 14
3.2. Single step co-electrodeposition method 17
4. Effect of electrodeposition potential 20
5. Effect of electrolyte pH 21
6. Effect of complexing agent concentration 22
7. Effect of sulfurization temperature and time 24
CHAPTER 3: EXPERIMENTAL TECHNIQUE 27
1. Fabrication techniques 27
1.1. Electrodeposition: 27
1.2. Cyclic voltammetry 30
1.3. Chronoamperometry 31
2. Characterization techniques 33
2.1. X-ray diffraction (XRD): 33
2.2. Raman spectroscopy 37

2.3. X-ray Photoelectron Spectroscopy (XPS) 40
2.4. Scanning electron microscopy (SEM) 43
2.5. Energy Dispersive X-ray Spectroscopy (EDS/EDX) 45
2.6. Photoluminescence (PL) spectroscopy 46
2.7. UV-visible spectroscopy 48
CHAPTER 4: RESULT AND DISCUSSION 51
1. Electrodeposition of Cu_2ZnSnS_4 thin films 51
2. Effect of deposition potential on the prosperities of CZTS thin films 56
2.1. Structural properties 56
2.2. Compositional and morphological analysis 61
3. Effect of Sulfur amount on CZTS thin films 70
3.1. Introduction 70
3.2. Structural properties 71
3.3. Compositional and morphological analysis 75
CHAPTER 5: CONCLUSION 84
FUTURE WORK 86
REFERENCES 87

LIST OF TABLES

Table 1: The calculations of the lattice parameters from (112) and (220) XRD peaks of CZTS thin films deposited at different potentials. 58

Table 2: The atomic percentage of CZTS thin films deposited at different potentials. 68

Table 3 : The atomic percentage of Cu, Zn, Sn, and S in the CZTS thin film sulfurized using different amounts of sulfur. 76

LIST OF FIGURES

Figure 1: The annual production and the price of the elements used in thin film solar cells. 3

Figure 2:The three crystalline structure of CZTS. 4

Figure 3: Isothermal section of the Cu_2S-SnS_2-ZnS system at 670 K. 6

Figure 4: A schematic structure of CZTS thin film-based solar cells. 7

Figure 5**:**(a) A schematic of p-n junction between layers (b) The band schematic of a p-n junction. 9

Figure 6: The four generations of solar cells. 11

Figure 7: The two methods of electrodeposition technique. 13

Figure 8: A schematic diagram of the stacked binary alloys. 14

Figure 9**:** A schematic diagram of the stacked binary alloys 14

Figure 10: A schematic diagram of single step electrodeposition method. 17

Figure 11: Schematics of a three electrode electrodeposition cell connected to a potentiostat. 28

Figure 12**:** A schematic of cyclic voltammetry. 31

Figure 13**:** Gamry reference 3000 device 32

Figure 14: X-ray diffraction schematics 34

Figure 15: X-Ray diffraction principle. 35

*Figure 16***:** A schematic shows the principle of Raman spectroscopy 38

Figure 17: Raman spectroscopy device. 39

Figure 18: Schematic of photoelectric process at electron energy levels. 41

Figure 19: A schematic of XPS working principle.....42

Figure 20: Types of electrons produced by an electron beam.....44

Figure 21: Schematic diagram shows the principle of EDS. 45

Figure 22: Energy diagram of PL process. 47

Figure 23: Photoluminescence *(PL)* spectroscopy *device.*.....48

Figure 24: Electromagnetic spectrum. 49

Figure 25: A volumetric flask contains the prepared solution. 52

Figure 26: Cyclic Voltammetry curve of CZTS electrolyte with 10 mV/s scan rate.....54

Figure 27: The tube furnace used in the sulfurization process. 55

Figure 28 : XRD analysis of the CZTS thin films deposited at different deposition potentials.....57

Figure 29: Raman analysis of CZTS thin films deposited at different potentials.....60

Figure 30 : XPS analysis of Cu in CZTS thin films deposited at different potentials. 62

Figure 31: XPS analysis of Zn in CZTS thin films deposited at diffenet potentials 63

Figure 32: XPS analysis of Sn in CZTS thin films deposited at different potentials.....64

Figure 33: XPS analysis of S in CZTS thin films deposited at different potentials.....65

Figure 34: EDS composition plot of sulfurized CZTS samples deposited at different potentials.....67

Figure 35 :The EDS spectrum of the CZTS sample deposited at -1.35V. 69

Figure 36: XRD analysis patterns of the CZTS thin films sulfurized using different amounts of sulfur as labeled. 72

Figure 37: Raman spectra of CZTS thin films sulfurized using different amounts of sulfur as labelled. 74

Figure 38: EDS analysis results of the CZTS films sulfurized using different amount of sulfur. 77

Figure 39: The EDS spectrum of CZTS sample sulfurized using 35 mg sulfur. 78

Figure 40: SEM cross section images of CZTS thin film on FTO coated glass substrate deposited using 35 mg sulfur. 79

Figure 41: Absorbance spectrum of CZTS thin film deposited at -1.35V and sulfurized using 35 mg sulfur. 81

Figure 42: $(\alpha h\upsilon)^2$ vs photon energy ($h\upsilon$) plot. 82

Figure 43: PL spectra of CZTS thin film deposited at -1.35 V and sulfurized using 35 mg of sulfur. 83

Figure 44: CZTS thin film solar cells structure. 86

CHAPTER 1: INTRODUCTION

1. Solar energy

Nowadays, the world is facing a growth in global population and human modernization, which increases the demand for energy consumption.[1] The fossil fuel such as coal, oil, and gas have been the main source of energy for human society, but it raised many issues and concerns. The fossil fuel has produced environmental pollution and climate changes due to the emission of greenhouse gases. Moreover, these fossil fuels are limited and will run out in the future. The development of renewable and clean energy sources such as solar energy, water, wind and biomass is important to address these energy concerns.[2,3] Solar energy is the most powerful and promising renewable energy source, and it is predicted that it will play an essential role over the next 60 years in electrical energy production.[4]

2. Photovoltaic (PV) technology and material

Photovoltaic (PV) is a term represents a clean technology which covers the conversion of sunlight directly into electricity. The development of photovoltaic devices can be divided into four generations.[1] The first generation is based on the single crystal Si which has a high efficiency, but it has a high cost. Thin film technology represents the second generation and it comes to overcome the high cost of crystal Si, however it reduces the efficiency of the solar cell. [2-3] The third generation contains various advanced technologies such as quantum dots [4] and dye sensitized solar cells[5]. Finally, the fourth generation covers inorganic hybrid materials such as perovskites[6]. In 2015, only 1% of the world's electricity was provided from PVs.[7]

3. Thin film solar cell

Thin film solar cells are mainly constructed of materials that strongly absorb sunlight. It reduces the demand for the row material were the thickness of the cell is varying from 1–3 μm. [3] There are many advantages of thin film solar cells such as the faster and cheaper manufacturing process. The absorption coefficient of thin film absorber materials is ~100 times higher than that of crystalline silicon.[3] The advantage of this is that a 100 times thinner layer of thin film material is required to absorb an equivalent amount of energy as crystalline silicon reducing manufacturing costs and price. In addition, thin film solar cells can also be fabricated on flexible substrate for instance metal foils or polyimides.[8] Another advantage is the adjustable band gap of the thin film materials, which can be done by varying the composition. Therefore, a large range of the solar spectra can be used and a higher efficiency is achieved.[9] Thin film PV devices have been recognized as a promising strategy to achieve high efficiency with low cost and thus satisfying the actual requirements of increasing electrical demand.

4. CZTS thin film solar cell

4.1.CZTS material

Recently, thin film technologies are based on CdTe or $CuInGaS(Se)_2$ (CIGS) light absorbers.[6] CIGS based solar cells has achieved high power conversion efficiency of more than 20%.[10] However, gallium, indium, and tellurium are expensive and rare elements. The use of cheaper, nontoxic, and abundant elements is important to develop an environmental friendly and economical materials. The elemental row materials prices and annual production is shown in figure 1.[11]

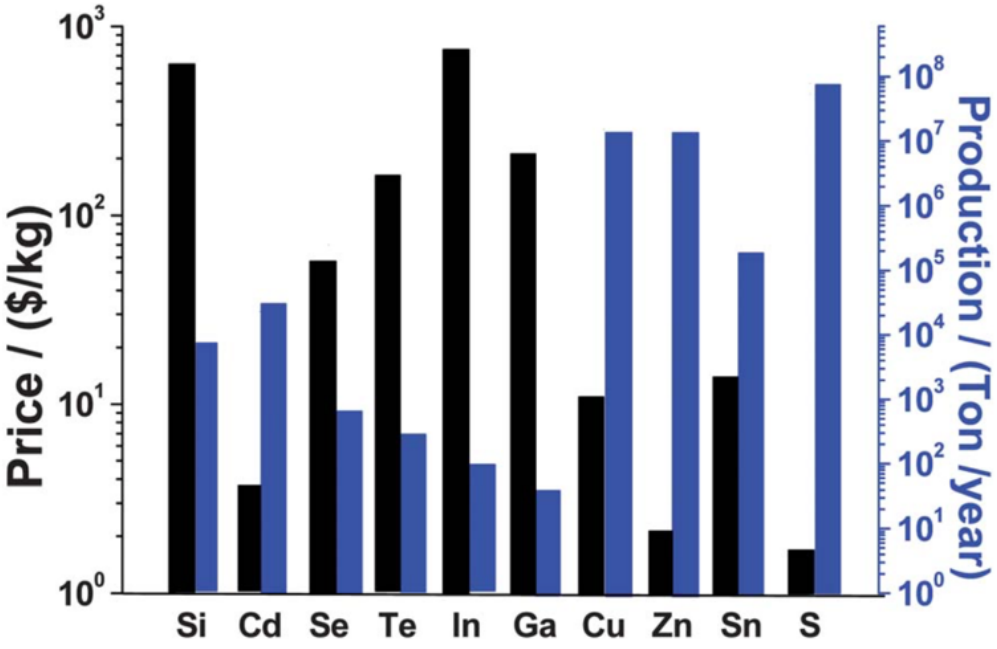

Figure 1: The annual production and the price of the elements used in thin film solar cells.

CZTS is a suitable alternative for CIGS were Zn, Sn and S are used to substitute In, Ga, and Se respectively. It is a quaternary compound semiconductor belongs to I_2-II-IV-VI_4 group and it was fabricated for the first time in 1974 by Schefer and Nitsche.[12] $Cu_2ZnSn(Se, S)_4$ is considered as a new light absorbing material for solar cell applications. This material has a tuned band gap were $Cu_2ZnSnSe_4$ has 1.0 eV and Cu_2ZnSnS_4 has 1.5 eV, and it can be tuned by controlling the amount of chalcogens in the material.[13]

CZTS material can be found in three types of crystal structures: kesterite, stannite and primitive mixed CuAu (PMCA). The kesterite and stannite are the same in structure and in Sn atom position. However, the difference between them is in the space distribution of Cu and Zn atoms within the unit cell as shown in figure 2.[14,14]

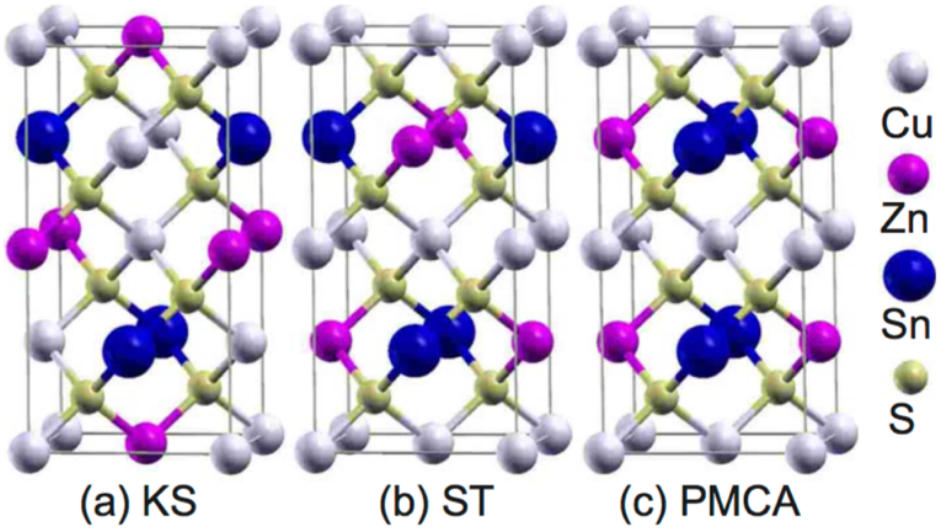

*Figure 2:*The three crystalline structure of CZTS.

The stannite and PMCA crystal structures are a CuAu like structure while the kesterite is derived from $CuInS_2$ (CIS). The kesterite structure shows more thermodynamically stable results when compared to the other phases. However, the challenge is in determining the phases, where their structures are similar and synchrotron light or neutron needed to identify them. There are a lot of arguments about CZTS structures. The first principles show that Cu_2ZnSnS_4 is most stable in kesterite structure, while some reports found it is in stannite structure.[15]

The theoretical efficiency of CZTS solar cells devices is 30%.[16] But, the thin film solar cells require a CZTS materials with a single phase kesterite material to reach a high efficiency.[16] Figure 3 expresses the isothermal section at 670 K of phase diagram for Cu_2S-SnS_2-ZnS system. The stable region of CZTS phase is in the center of the phase diagram, and the pure phase has a small compositional range at this temperature. A secondary phases forms outside of this region besides CZTS primary phase. The formation of the impurity phases can affect the properties of the material which leads to a low performance of the cell. The creation of these phases can play an important role in the recombination centers and the charge collection barriers that lower the performance of the cell. The experimental results proposed that the zinc-rich and copper poor CZTS thin film with Cu/(Zn+Sn) = 0.8 and Zn/Sn = 1.2 is the best composition to achieve a good performance solar cell.[17-20]

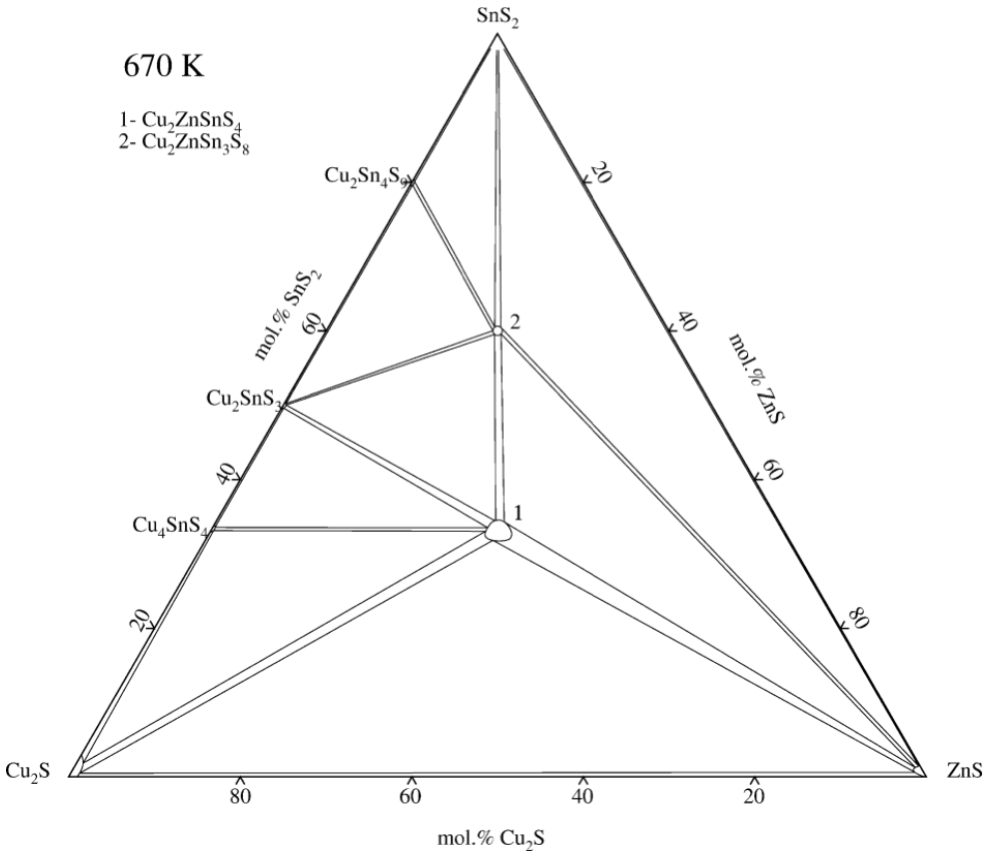

Figure 3: Isothermal section of the Cu_2S-SnS_2-ZnS system at 670 K.

4.2.Structure of CZTS absorber layer for solar cells

Thin film solar cell involves a front and back metals considered as an electrical contacts, a window layers, p-type thin film absorber layer, and n-type buffer layer. Figure 4 shows the structure of solar cell were CZTS thin film act as an absorber layer. The CZTS thin film (1~2 μm thick) is deposited on a substrate such as FTO coated glass which acts

as a back electrical contact. CdS is an n-type semiconductor and acts as a buffer layer which is coated by chemical bath deposition. Finally, the window layer and a contact are deposited by sputtering.[21-22]

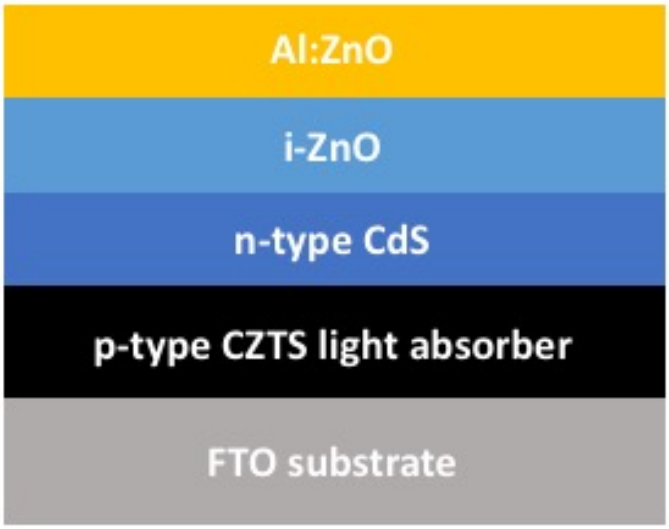

Figure 4: A schematic structure of CZTS thin film-based solar cells.

4.3.Working principle of CZTS absorber layer for solar cells

In solar cell device, the crucial part is the p-n junction which is made between the p-type and n-type layers. The p-type is a conducting layer for holes, while the n-type conducting layer is for electrons. When an electron of the absorber layer absorbs a photon with an energy equivalent or higher than the energy of the band gap, the electron is excited and generates an electron-hole pair or exciton.[23] A difference in chemical potential between electron and hole will exist, and a separation between them will be generated at the p-n junction. The charge carriers will drift in opposite directions and the electrons and holes will be injected in the external circuits to generate current. If the photons has a less energy than the energy of the band gap it will not be absorbed and it will be considered as a loss due to their failure to create electron-hole pair. The photons with higher energy can be absorbed but a portion of the energy could be lost as heat.[23] The process at the p-n junction is showed in figure 5 .[24]

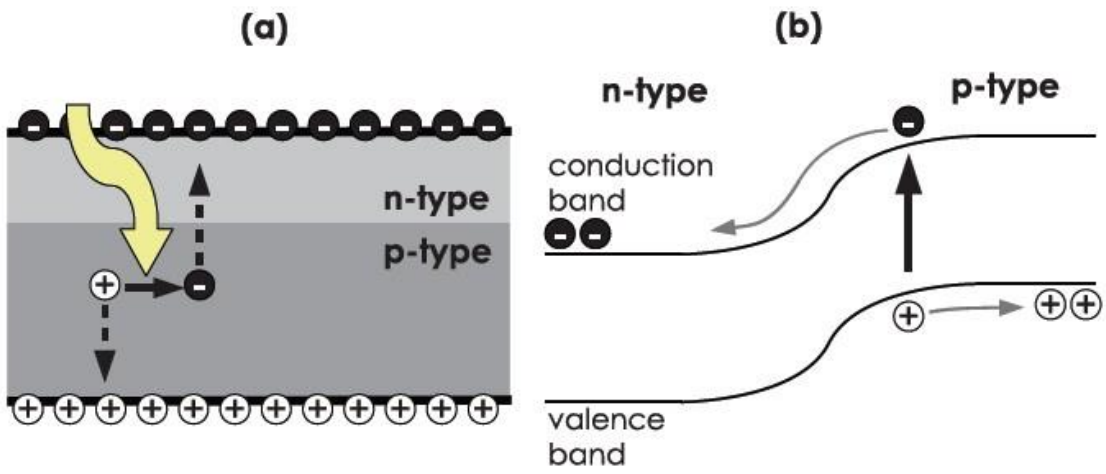

Figure 5:(a) A schematic of p-n junction between layers (b) The band schematic of a p-n junction.

In this work, we use single step electrodeposition technique to deposit CZTS absorber layer for solar cell application. Then, we report the effect of sulfur amount in the sulfurization process on the CZTS thin film. This thesis is represented in five chapters. The first chapter is an introduction to solar energy, solar cells generations and CZTS thin film solar cells. The second chapter is the literature review which covers the previous efforts which are done on CZTS material. The experimental tools and the characterization technique were explained in the third chapter. In the fourth chapter the results are presented along with the related discussion. The conclusion and the future work will be in the fifth chapter.

CHAPTER 2: LITERATURE REVIEW

1. Solar cells generations

Solar cells technologies are divided into four main generations and its shown in figure 6. The solar cells first generation is constructed on crystalline silicon, which demonstrate a performance around 15-25%. In 2014, Masuko et al. accomplished the a maximum efficiency of 25.6% by using crystalline silicon heterojunction.[25-26] This type of solar cells rule the market due to their excellent performance. However, This type is very rigid and it also required a lot of energy in the production process.

The second generation of solar cells is the amorphous silicon[26], CIGS[27] and CdTe[28]. The performance of these materials is 10-20%, but its came to avoid the high cost of crystalline silicon solar cells. These types of solar cells has a low materials consumption and low production cost. In addition, the second generation of solar cells are fixable and can be produced. However, the vacuum processes and the high temperature treatments cause a large energy consumption. The highest efficiency achieved for amorphous silicon is 14.6%. In 2010, the highest efficiency of 20% for CIGS was achieved by Philip et al.. In their work, they demonstrate a high reproducibility by analyzing the main characteristic of solar cell from the performance level. [29] On the other hand, CdTe achieved an efficiency of 16.5% by Xuanzhi Wu by developing a two manufacturing processes.[30]

The third generation contains many advanced technologies such as quantum dots[4] and dye sensitized [5] solar cells and these solar cells achieved about 5-15% energy performance. Michael Gratzel reached 12% current conversion efficiency using the dye sensitized solar cells[31], while Yuh- lang et al. reach 4.22% for quantum dot. [32]

Finally, the fourth generation is the inorganic hybrid materials such as perovskites[6] and

this type of solar cells obtained 22.7% efficiency by Sang et al. in 2018. [33]

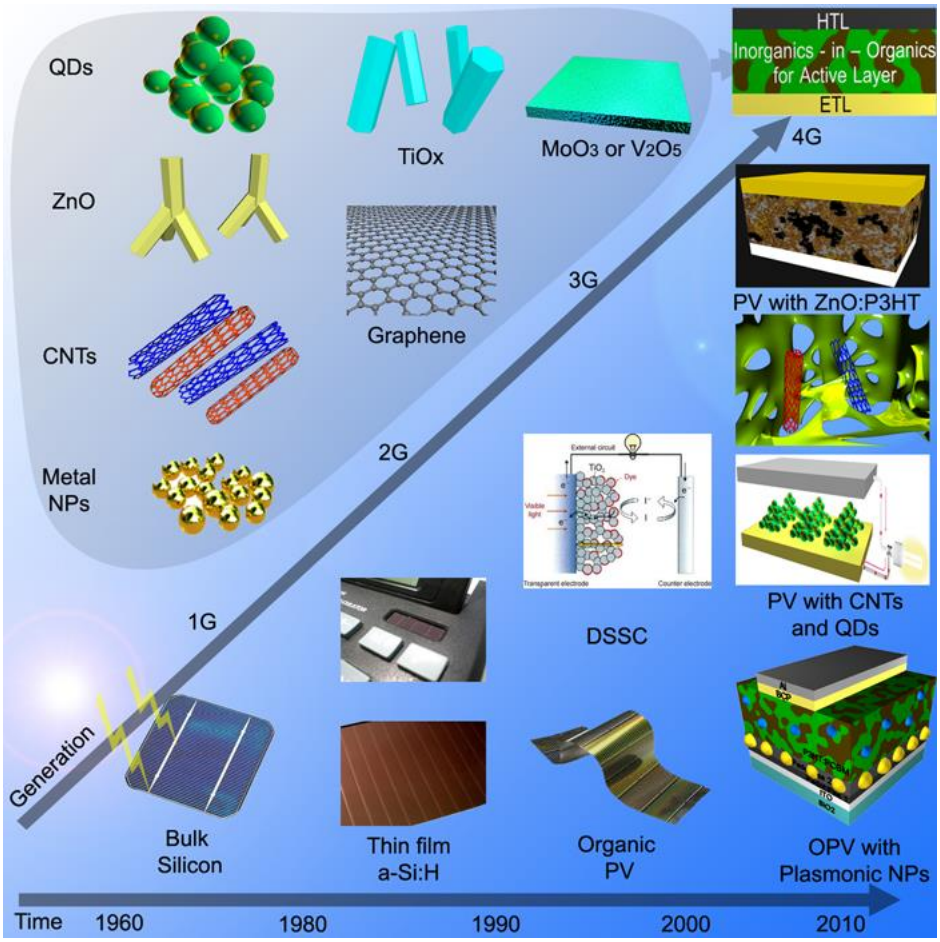

Figure 6: The four generations of solar cells.

2. CZTS Thin film

CZTS (Cu_2ZnSnS_4), CZTSe ($Cu_2ZnSnSe_4$)[34] and CZTSSe ($Cu_2ZnSn(Se, S)_4$)[35] thin films have been a place of interest in the last years. These materials achieved a power conversion efficiency of 9.2%[36], 11.6% and 12.6 %, respectively. CZTS is an ideal material for solar cell applications because of its suitable band gap (1.4-1.6 eV) and the high adsorption coefficient (10^4 cm^{-1}). The photovoltaic response of CZTS material was first reported in 1988 by Ito and Nakazawa. It was based on the creation of a junction between CZTS absorber layer and a buffer layer on a stainless steel substrate. They fabricated the film by argon beam sputtering technique and the device recorded an open circuit voltage of 165 mV. The band gap of CZTS was determined and it was 1.45 eV, which is an ideal value for an absorber layer in solar cell applications. [37]

These thin films can be fabricated using different techniques which can be classified into two main categories[38-39]: vacuum based method and non-vacuum based method. The vacuum based method such as sputtering[40-45], pulsed laser deposition[44, 46-47] and evaporation[19, 48-50]. These methods can produce a high uniform CZTS thin films which make the film controllable and reproducible. However, they need high-energy consumption and long deposition time. The non-vacuum based methods established to overcome these problems and provide a low cost and a rapid production of CZTS thin films. This technique includes chemical vapor deposition[51-52], spray pyrolysis[53-58], spin coating[59-60] and electrodeposition[61-64]. In this paper, a review will be done on CZTS thin films synthesized by electrodeposition technique. The study will include the CZTS material properties, crystal structure and electrodeposition preparation technique. Many critical factors

influence the formation and composition of CZTS thin films such as the applied potential, electrolyte PH, and sulfurization temperature and sulfurization time.

3. Electrodeposition technique:

CZTS thin film have been fabricated using different deposition methods and electrodeposition is one of them. This technique is one of the most attractive methods in solar cell absorber layer production. As compared to non-vacuum based technique, the highest efficiency of 8.1% was achieved using electrodeposition. Electrodeposition is an environmentally friendly and low cost method and it is applied for the growth of many absorber layers such as CIGS and CdTe. The fabrication of the CZTS thin film using electrodeposition can be done by one of two ways, which are (i) the stacked elemental layer or binary alloys; (ii) single step co-electrodeposition. Figure 7 below shows the two methods of electrodeposition technique.

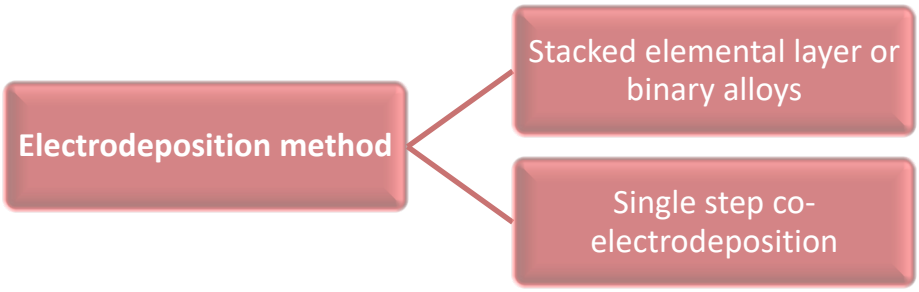

Figure 7: The two methods of electrodeposition technique

3.1. Stacked elemental layer (SEL) or binary alloys

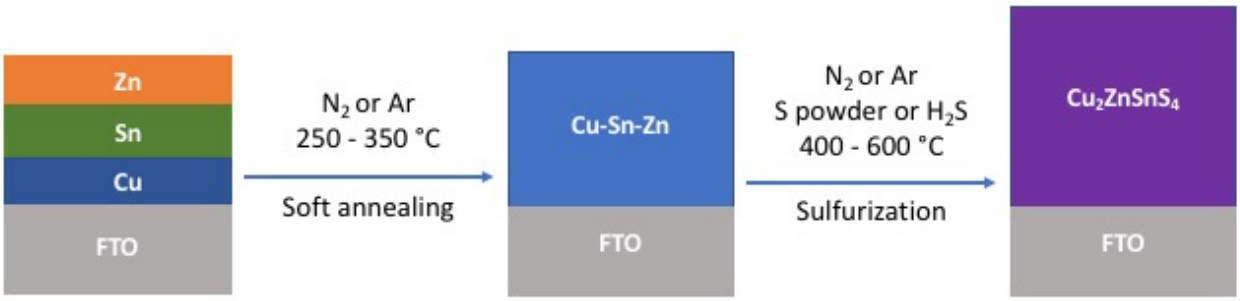

Figure 8: A schematic diagram of the stacked binary alloys.

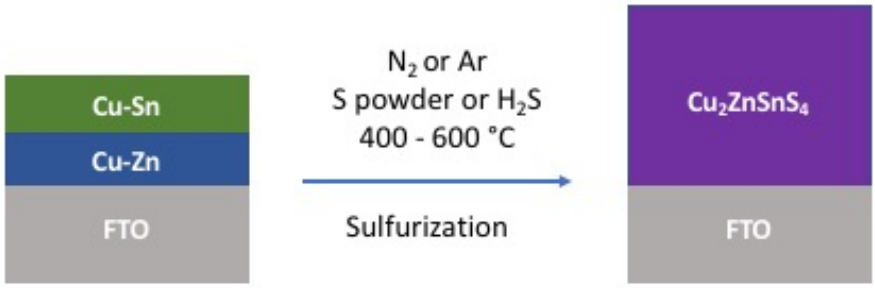

Figure 9: A schematic diagram of the stacked binary alloys

In this method, copper, zinc and tin are subsequently deposited from an electrolyte solution. The first electrodeposition of CZTS thin film was reported by Scraag et al. with 0.8% efficiency.[65] The deposited film was Cu/Sn/Zn metal stacks on Mo substrate followed by sulfurization at 550 °C for 2 h. They related the low efficiency to the formation of voids near the CZTS and Mo interface, and the formation of secondary phase as a result of zinc deficiency. They enhanced the deposition process by using Cu/Sn/Cu/Zn sequential stack, and using KCN etch to eliminate the Cu_xS phase which gives higher efficiency of 3.2%.[66-67]

Sequentially electrodeposition of CZTS thin film was reported by IBM group in 2012 with an efficiency of 7.3%. The group sequentially deposited Cu/Zn/Sn stacks followed by annealing at a low temperature between (210-350 °C) under N_2 atmosphere. The annealing step is done in order to produce a homogeneous and highly crystalized metallic layer.[68-69] The final step is the annealing of the alloys for 5-15 min at 550-590 °C in a sulfur atmosphere to allow the formation of CZTS material. The results show the presence of various secondary phases when the sulfurization temperature is below 580 °C. At a temperature higher than 580 °C, ZnS and Cu_2SnS_3 secondary phases reacts and CZTS formed. The highest efficiency of 7.3% was found by fabrication of CZTS thin film solar cell that were sulfurized at 585 °C for 12 min. [22, 70]

In 2014, Lin et al. reported the synthesis of CZTS absorber layer by using stacked elemental layer technique. CZTS absorber layers were obtained by the sulfurization of the metallic layer Cu-Sn-Zn in an inert atmosphere. The film was preheated for 20 min at 350 °C before the sulfurization and it was found that the film exhibits no secondary phases,

uniform and densely packed surface with no crevices or voids. The solar cell with an Al:ZnO/CdS/CZTS/Mo structure were fabricated from a metallic precursor was preheated for 20 min at 350°C and it shows a conversion efficiency about 5.6%.[71]

The highest efficiency for pure CZTS-based solar cell that are fabricated using sequential electrodeposition technique in 2015 by Feng Jiang et al. [69] They produced the CTZ precursor by using stacked elemental layer followed by heating for 200 min and sulfurization at high annealing temperature. The efficiency of the solar cell was determined to be 8.1%.[69]

In order to prepare the stacked metals, different orders of three metals can be used. The reports show that the Cu/Sn/Zn is the ideal sequence of deposition that gives a high performance CZTS thin film solar cell.[22, 71] The sequence results in a good metal exchange and stabilization of metal layers.[72]

In stacked binary alloy method the precursor alloys Cu-Sn and Cu-Zn are electrodeposited on a substrate. The sulfurization of the precursor will result in the formation of CZTS thin film. Yuan et al. [73] reported this method for the first time where CZTS thin films fabricated by the sulfurization of sequentially electrodeposited stacked binary alloys Cu-Sn and Cu-Sn. The sulfurization was done using 0.05 Mpa sulfur at 580°C for 30 min. The solar cells device with the structure of ITO/i-ZnO/CdS/CZTS/Mo/Glass showed an efficiency of 3.67%. The high series resistance and recombination rate were a limiting factors for the efficiency. [73]

3.2.Single step co-electrodeposition method

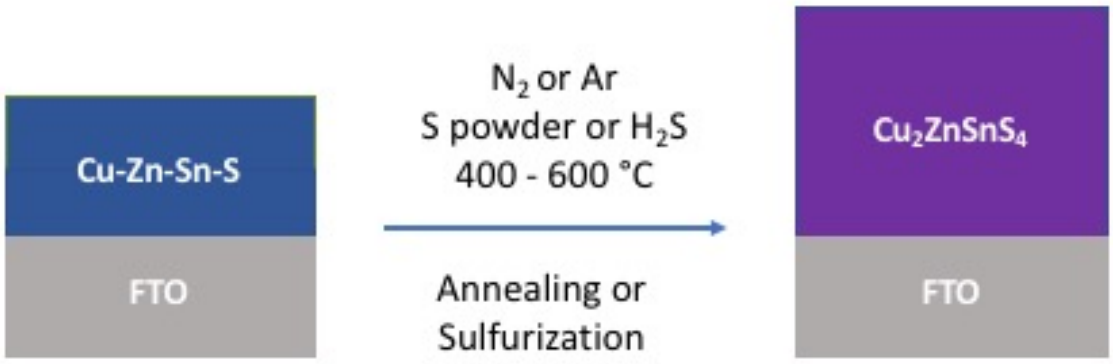

Figure 10: A schematic diagram of single step electrodeposition method.

In this method the precursor film Cu/Zn/Sn is deposited from a deposition path contains Cu, Zn and Sn cations. The deposition is followed by sulfurization process using sulfur source for instance pure S vapor, S2+N_2 and S_2+Ar.

In 2009, Ennaoui et al. [74] introduced the single bath electrodeposition of CZTS thin films. The deposition of Cu/Zn/Sn precursor layer on Mo glass substrate was done by using an alkaline electrolyte bath contain Cu (II), Zn (II) and Sn (IV) metal salts. The precursor

was then annealed at 550 °C for 2 hours in Ar-H_2S atmosphere. The results showed that CZTS thin film with Cu/(Zn+Sn)= 0.97 and Zn/Sn = 1.08 has the best efficiency of 3.4%.[74]

Using the same electrodeposition method, Araki et al.[75] (2009) reported the synthesis of CZTS thin films . The Cu/Zn/Sn film was annealed in sulfur atmosphere for 2 hours at 600°C. The Zn rich film gives the highest efficiency of 3.16%. The electrodeposition electrolyte was prepared by using copper (II) sulfate, zinc sulfate, tin (II) chloride and tri-sodium citrate. After annealing, the co-electrodeposited film didn't show any phase separation.[75] In addition, Li et al. fabricated CZTS thin film using co-electrodeposition of Cu/Zn/Sn precursor with 3.62% power efficiency.[76]

Rakhshani et al.[77] electrodeposited CuZnSn metallic alloy film on Mo substrate from Zn rich electrolyte. The precursor films were sulfurized in sulfur atmosphere then characterized using different characterization techniques. X-Ray Diffraction and Raman spectroscopy were used to identify the crystal structure of the film, while the uniformity of the films were observed by scanning electron microscopy. The results proved the formation of Cu_3Sn, Cu_6Sn_5 and Cu_5Zn_8 phases in the precursor thin film. The XRD and Raman results after the sulfurization confirmed the conversion of precursor films to Cu_2ZnSnS_4. A heterojunction diodes between CdS/ Cu_2ZnSnS_4 were fabricated and the diodes showed a good ideality factor of 1.3-1.9, current rectification factor of ~120, and reverse biased saturation current of ~30-60 $\mu A/cm^2$. [77]

In 2010, Power et al. demonstrated a single step co-electrodeposition where the electrodeposition of S is done with the metals. The electrodeposition was done at room

temperature using $CuSO_4$, $ZnSO_4$, $SnSO_4$, and $Na_2S_2O_3$ (sulfur source) in an electrolyte solution bath. The deposition of the film followed by annealing for 1hour at 550 °C in Ar atmosphere. The band gap of the film was found to be 1.5 eV.[78] Some reports showed that to fabricate a high quality CZTS thin film additional sulfur source is necessary in the annealing process such as S powder or H_2S.[79]

S.G. Lee et al.[80] fabricated a CZTS absorber layer for solar cell application by using the single step electrodeposition technique. The film was deposited at 1.05 V followed by annealing at high temperature in sulfur atmosphere. The XRD analysis of as-deposited samples showed an amorphous structure, but the CZTS thin film was obtained after the sulfurization of the as- deposited films from 450 to 580 °C. The as-deposited samples showed voids along with agglomerated particles, while after sulfurization, the samples become more uniform and dense. The band gaps of the samples after sulfurization were found in the range from 1.9 to 1.5 eV. [80]

MG et al. (2016) synthesized a high quality CZTS thin film using single step electrodeposition method.[81]The thin film was deposited from an electrolyte containing $CuCl_2$, $ZnCl_2$, $SnCl_4$ and $Na_2S_2O_3$ on FTO coated glass substrate. The deposition potentials of the films was -1.1 V vs. Ag/AgCl reference electrode. The CZTS layers were annealed for 15 minutes at 400°C . The XRD results revealed the presence (112), (220) and (312) planes which are related to the CZTS kesterite phase. From UV-visible Spectroscopy and Photoluminescence, the band gap of the films were estimated to be ~ 1.49 eV. Upon the heat treatment, the grain size has been increased and the current density-Voltage

measurements revealed a Schottkey behavior. C-V measurements were used to estimate the flat band potential and carrier concentration CZTS thin films and it was 0.30 V and ~ 2.4 x 10^{16} cm^{-3} respectively.

In 2017, Aiyue Tang et al. reported a novel green electrolyte which is designed for the synthesizing of CZTS thin films with high S content. The one-step electrodeposition was done using K_4P_2O7 and $C_7H_6O_6S$ which are added to act as a complexing agent in the electrolyte. The results showed that the as-deposited film had a high S content which satisfy the stoichiometry. The as-deposited film was annealed at high temperature and a continuous and uniform CZTS thin film was obtained. The produced CZTS thin film had a pure kesterite structure and a suitable band gap of 1.53 eV. The study showed that the presence of $K_4P_2O_7$ prevented the excessive deposition of Cu^{2+} and Sn^{2+},while the $C_7H_6O_6S$ promoted the reduction of Zn^{2+}.[82]

There are different parameters that affect the properties of the formed CZTS thin film such as the pH of electrolyte solution, deposition potential and the concentration of the complexing agent. Also, the sulfurization process is affected by the sulfurization temperature and time.

4. Effect of electrodeposition potential

The effect of potential is very important as the electrolyte have various reduction species which needs to be reduced at a specific potential. The effect of electrodeposition potential was reported by different groups where they investigated the effect of deposition potential on the as-deposited film to understand the growth behavior and improve the film

quality.[83-84]

Ananthoju et al. [85] examined the compositional, structural and the optical properties of the CZTS films. The films were deposited at different potentials of -1.0, -1.2, -1.4, -1.6, -1.8 and -2.0 V with respect to Ag/AgCl. After the deposition, the films were sulfurized at 550 °C for 30 min in argon atmosphere. The results showed that the deposition at -1.4 V vs. Ag/AgCl resulted in the best film quality. XRD and Raman spectroscopy analysis of the film showed a highly pure crystalline CZTS kesterite phase. EDS and XPS showed an ideal stoichiometric compound for the film deposited at -1.4 V. [85]

5. Effect of electrolyte pH

Different groups studied the effect of pH on the quality of CZTS thin film using different complexing agents and glass substrates. In 2013, M. Coa et al. [86] investigated the effect of pH value on the formation of CZTS thin film. Mo-glass was used as a substrate and $Na_2EDTA$was used as a complexing agent. The best results were obtained in pH between 3.5-4.0 where the produced film consists of kesterite phase CZTS. The band gap was of ~1.48 eV and 0.30% conversion efficiency was achieved.[86]

Two studies were performed using tri-sodium citrate as a complexing agent but on different substrates. In the first study Hong Zhang et al. used co-electrodeposition method to prepare CZTS thin film from electrolytes with different pH values. They used FTO glass as a substrate and it was found that the pH value influence the reduction potential of the used metals which leads to off-stoichiometric in the deposited films. When the bath pH value is about 5, the XRD and Raman analysis show that the final CZTS thin films have a

better crystallinity and less secondary phases. CZTS thin films fabricated at pH = 5 had a stoichiometric composition and a bandgap energy around 1.49 eV.[87] The other study was reported by Amrut Agasti et al. [88] where Mo-coated glass was used as a substrate. The co-electrodeposition of the precursors were performed using electrolytes of pH varying from 4 to 8. The CZTS thin film deposited at pH = 6 showed a dense morphology with phase purity and suitable band gap (1.45 eV).[88]

Lately, The deposition of CZTS thin film on indium tin oxide (ITO) substrate at different pH was reported by R. Sani et al. With the increase in the pH of the electrolyte the deposition potential were found to move in the anodic direction. The analysis shows that the deposited CZTS thin film formed at pH = 2.5 is closer to the required stoichiometry of 2:1:1:4. [89]

6. Effect of complexing agent concentration

In electrodeposition of CZTS thin film, it is necessary to add a complexing agent to the electrolyte in order to narrow the potential gap among the elements. The presence of the complexing agent in the electrolyte throughout the electrodeposition of the precursor improves the quality of the film and the life time of the deposition bath. The tri-sodium citrate is the most attractive complexing agent, and many groups reported the effect of its concentration in the electrolyte.

Power et al. [90] (2010) investigated the effect of tri-sodium citrate concentration on the structural and compositional properties of CZTS thin films. CZTS thin film electrodeposited on Mo-coated glass substrate using an electrolyte with pH (4.5-4) at room

temperature. The as-deposited film prepared without using tri-sodium citrate showed a well-covered surface morphology with some cracks on the surface. Whereas the films prepared using the tri-sodium citrate revealed non uniform and porous surfaces, but the morphology changed after annealing. The films were uniformly distributed over surface of the substrate. The analysis shows that best stoichiometric can be found by using 0.2 M tri-sodium citrate. [90]

Jeon et al. [91] (2011) explored the morphological, structural and compositional characteristics of CZTS thin films deposited using single step electrodeposition. The results showed that with increasing the complexing agent volume in the solution, the grain sizes of CZTS thin films became smaller. The best stoichiometric were observed by using the volume of 25 mL tri-sodium citrate and the XRD analysis confirmed the kesterite structure. [91]

Remarkable comparison between three complexing agents which are tri-sodium citrate, ethylenediamine tetraacetic acid and tartaric acid has been reported by Mkawi et al. in (2014). The effect of these complexing agents on the properties of CZTS thin film were studied. From the cyclic voltammetry, it was found that tri-sodium citrate is a suitable complexing agent due to its ability to align the deposition potentials of Cu, Zn, and Sn. The analysis of the films confirmed the suitability of tri-sodium citrate. The fabricated solar cells achieved a conversion efficiency of 2.9%.[92]

7. **Effect of sulfurization temperature and time**

The sulfurization process can affect the properties of the produced CZTS thin film. The sulfurization temperature and sulfurization time considered as an important parameters that influence the morphological, structural and compositional characteristics of CZTS thin film.

In 2009, Araki et al. investigated the influence of sulfurization temperature on CZT thin film deposited on Mo coated substrate by staked elemental layers method. The deposited films were sulfurized at different temperatures 300, 400, 500 and 600°C in nitrogen gas atmosphere. The results showed that CZTS kesterite phases were detected by the sulfurization of precursor at temperature above 400°C. The open circuit voltage and the short-circuit current were measured for the CZTS thin film sulfurized at 600°C and found to be 262 mV and 9.85 mA/cm^2, respectively. While the efficiency of the cell was 0.98%.[75, 93]

Lately, Mkawi et al. reported the effect of the temperature used in the sulfurization process of the CZT precursor on the properties of the CZTS thin film. The thin films were fabricated by electrochemical deposition technique, while the sulfurization temperature were controlled between 250 and 400°C. XRD and Raman measurements proved the presence of the kesterite phase of CZTS. It was observed that there is an increase in the grain size and crystallinity of the CZTS films with increasing the temperature in the sulfurization process . There was a variation in the absorption coefficients and the band gaps of the films due to the difference in the sulfurization temperature, where it was in the

range of 3–4.1x 10^{4} cm^{-1} and 1.4–1.53 eV, respectively. The fabricated photovoltaic device with CZTS thin film sulfurized at 400°C revealed a maximum efficiency of 2.04 %. This efficiency was attributed to the higher crystallinity of the film and larger grain size of CZTS compared with those sulfurized at lower temperatures.[94] The same group investigated the effect of the sulfurization temperature on CZTS thin film but by using a higher temperature range. The sulfurization temperatures were 460, 500, 540 and 580 °C and it was found that CZTS thin film sulfurized at 580 °C exhibited the best characteristics with an efficiency of 2.69%.[95]

The effect of sulfurization time on CZTS thin film was studied in 2013 by Guan et al. The effect of sulfurization time on structure, composition and other properties of these CZTS thin films were investigated. The sulfurization times were 20, 40, 60, 80 and 100 min. The results indicate that a secondary phase exists in the CZTS thin films sulfurized for 20-40 min. The band gap ranges from 1.49 to 1.56 eV. The best result was achieved by sulfurization for 80 min. The film exhibited a single kesterite structure and an ideal band gap 1.55 eV with a high absorption coefficient 10^{4} cm^{-1}. [96]

A present study on the effect of sulfurization time was conducted by Aldalbahi et al. CZTS thin films were prepared by electrodeposition technique. The effect of sulfurization time 75, 90,105 and 120 min on the properties of CZTS thin film was studied. The film sulfurized for 120 min exhibited the best results where the analysis confirmed the formation of CZTS kesterite phase and the stoichiometric composition.. The band gap of the films were between 1.37–1.47 eV. [97]

However, the effect of sulfur amount on CZTS thin film deposited on FTO coated glass substrate by using single step electrodeposition technique has not been reported yet.

CHAPTER 3: EXPERIMENTAL TECHNIQUE

1. Fabrication techniques

1.1. Electrodeposition:

Electrodeposition is a non-vacuum technique that is low in cost, environmentally friendly, and it scales well from small area deposition in laboratory to large area. Therefore, electrodeposition considered as a prospective technique toward industrial level for commercial mass production. The electrodeposition method works at room temperature and does not require an excessive amount of energy. On the other hand, vacuum technology involve the use a high energy in order to create the vacuum condition.[20]

Electrodeposition is an electrochemical process that uses electric current to reduce metal cation dissolved in an electrolyte to form a metal coating on an electrode. Figure 11 shows a schematic diagram of an electrochemical cell consists of three electrodes. The working electrode which is the cathode, The counter electrode which is the anode and the reference electrode. The electrodes are dipped in an electrolyte bath containing a certain concentration of metal ions and connected to a potentiostat to monitor and control the applied voltage. The voltage is applied at the cathode and measured with respect to the reference electrode. In the electrodeposition process the metal ions are reduced at the cathode-electrolyte interface and combined with the growing metal film.

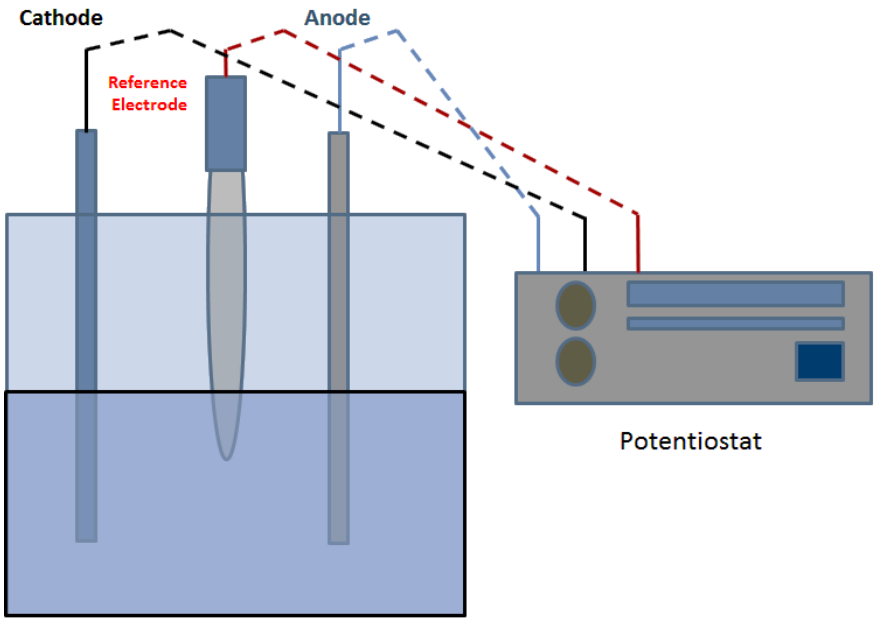

Figure 11: Schematics of a three electrode electrodeposition cell connected to a potentiostat.

The reduction of the metal ion Me^{z+} in the solution is represented by the following reaction,

$$Me^{z+} + ze^{-} \rightarrow Me \qquad (1)$$

If a complexing agent L is used in the solution the reaction will be represented as follows,

$$[Me_xL_y]^{z+} + ze^{-} \rightarrow xMe + yL \qquad (2)$$

The role of the complexing agent is based on the decrease of the effective concentration of metal ions and enables the tailoring of the redox potential by binding to the metal ions. These reactions occur at the electrode-electrolyte interface. When the cathode is immersed in the electrolyte an equilibrium occurs between the metal ions in the solution and the metallic atoms at the electrode. This equilibrium produces a voltage drop between the cathode and the electrolyte, generating a separation of charges and forming a double layer. An interface charge layers are formed under these equilibrium conditions and two types of processes can happen upon applying a potential. The first type is the Faradaic processes, where the electrons are transferred across the electrode-electrolyte interface to enable the oxidation or reduction reactions based on Faraday's law. The second type is the non-faradic processes, in this process the structure of the double layer can change due to adsorption or desorption of ions or molecules which is dependent on the applied potential. In faradaic processes, Nernst equation is used at equilibrium :

$$Eeq = Eo + \frac{RT}{zF} \ln a\,(M^{z+}) \qquad (3)$$

where E_O is the standard electrode potential, R is the gas constant, F is the Faraday constant, a is the activity of metal ions, and z is the numbers of electrons involved in the reaction. The equilibrium is dynamic at this value of electrode potential and the overall current is zero. To reduce the metal ions in a solution, a potential more negative than the Nernst potential must be applied to generate a driving force.[98]

1.2.Cyclic voltammetry

Cyclic voltammetry is an important and basic electroanalytical technique used to analyze redox systems on a working electrode surface. The reduction and oxidation processes can be estimated by analyzing a signal current changes as a function of potential. In electrodeposition of metals or metals alloys this technique is used to distinguish the reduction potentials of the metals cation in the electrolyte bath. The scan rate is the rate of voltage change over time during the experiment. The potential is measured between the reference and the working electrodes, while the measurements of current is between the counter and the working electrodes. This records are then plotted as current versus the applied potential.[99]

A cyclic voltammetry graph is shown in figure 12 and it is obtained by measuring the current at the working electrode throughout the potential scans. The figure represents the cyclic voltammetry plot resulting from an electrode reduction and oxidation based on the following reversible reaction of the metal ion M^+

$$M^+ + e^- \rightleftharpoons M \qquad (4)$$

By scanning the potential negatively, a reduction reaction occur and the resulting current is the cathodic current i_{pc} and the corresponding peak potential is called the cathodic peak potential E_{pc}. The oxidation reaction will occur when the potential is scanned positively, where i_{pa} and E_{pa} are the anodic current and the anodic peak potential, respectively.[100-101]

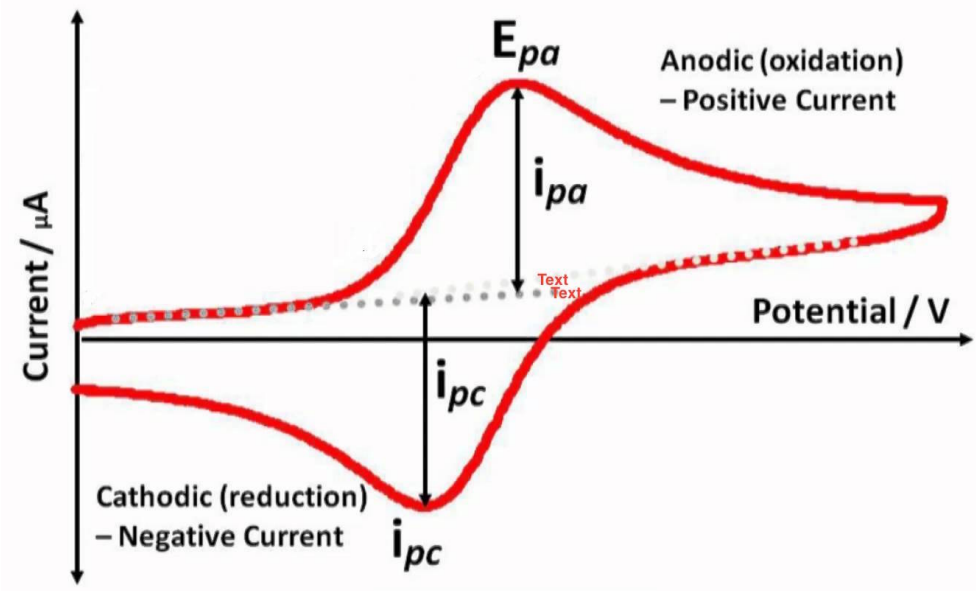

Figure 12: A schematic of cyclic voltammetry.

1.3.Chronoamperometry

Chronoamperometry is an important electrochemical technique where the change in current at the working electrode is recorded as a function of time under applied potential. This technique is used to study the nucleation and electrodeposits material. In addition, it can be used to identify the changes in surface area during electrodeposition processes.

Chronoamperometry is considered as a time dependent method, where a fixed potential is applied to the working electrode. In this technique, the current is measured as a function of time, according to the diffusion of the analyte from the solution to the surface of the sensor. Therefore, chronoamperometry can be used as a measuring technique of

time- current dependence for a process with a diffusion controlled occurring at the electrode surface.

In this work, Gamry Reference 3000 potentiostat/Galvanostat /ZRS was used to perform the electrochemical tests. The device is shown in figure 13.

Figure 13: Gamry reference 3000 device

2. Characterization techniques

Various measuring techniques were used to determine the properties of the prepared film. X-ray diffraction (XRD), X-ray photoelectron spectroscopy (XPS) and Raman were used to determine the crystallinity of the film and to check the formation of the required structure. The surface topography, morphology and the film thickness were determined using scanning electron microscope (SEM). The film stoichiometry was determined by energy dispersive X-ray spectroscopy (EDX) . UV-visible spectroscopy and photoluminescence (PL) spectroscopy were used in the measurement of the band gap.

2.1. X-ray diffraction (XRD):

X-ray diffraction is one of the most important techniques in crystal structure studying among the various science fields such as chemistry, physics and material science. The crystalline properties of a material such as crystalline structure and lattice constants can be determined using this characterization method. XRD setup consists of x-ray source, sample holder, goniometer and a detector, shown in figure 14.

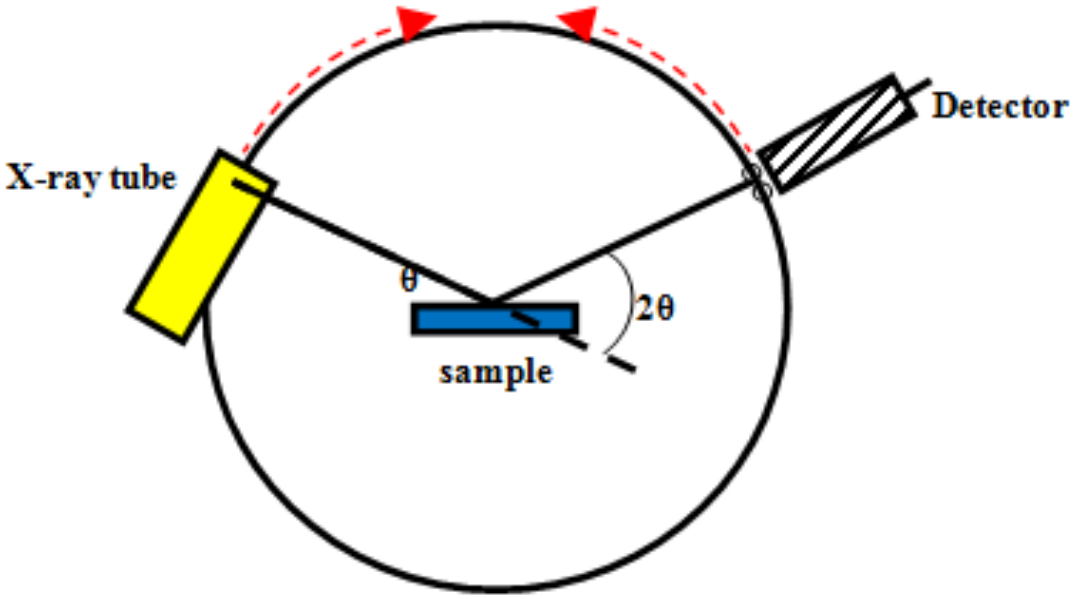

Figure 14: X-ray diffraction schematics

The XRD principle is based on Bragg's law where the x-rays wavelength is related to the crystal lattice spacing and diffraction angle. In the XRD, the X-rays are focused at the sample and the diffracted rays are detected. These rays are interfering out of a definite crystalline planes in a certain direction (diffraction angle) as shown in figure 15. Bragg's law is given as follows:

$$n\lambda = 2d_{hkl}\sin(\theta) \qquad (5)$$

where n is reflection order, λ is the x-ray wavelength, d_{hkl} is the spacing between the planes, hkl are Miller indices and θ is scattering angle.

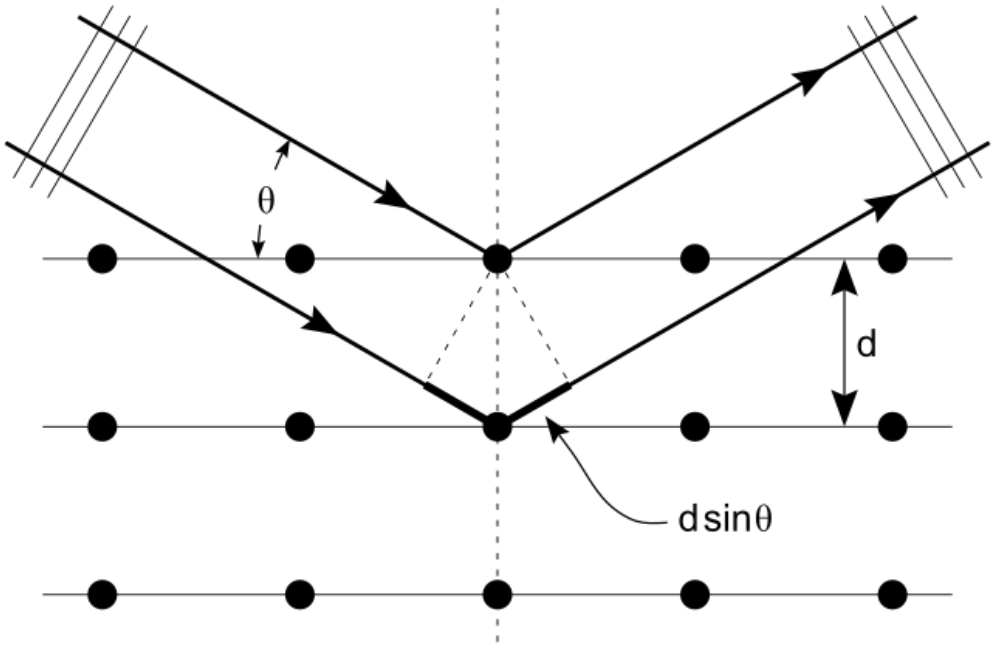

Figure 15: X-Ray diffraction principle.

X-rays are usually produced by a cathode ray tube then it is filtered in order to generate monochromatic radiation. The x-rays are formed under vacuum where electrons are produced using a high current by a heated filament. The free electrons are accelerated by high voltage toward the anode and the interactions between them generate x-rays. The produced x-rays will be concentrated and directed toward the sample. When the conditions satisfy Bragg's law, the interaction between the incident x-ray and the crystalline material will produce a constructive interference and diffracted rays. Finally, the diffracted rays are detected and counted. [102-103]

In addition, the crystallite size and lattice strain can be determined from the XRD analysis. The main sources of diffraction peak broadening are broadening from the instrument, crystallite size and lattice strain in the material due to crystal imperfections and defects. XRD is a powerful tool to measure the crystallite size and strain in the material.[104-105] In Williamson-Hall (W-H) analysis the contributions of both of the strain and crystallite size towards line broadening are considered. The instrumental broadening is corrected using the following formula

$$\beta_{hkl} = \left[(\beta_{hkl})^2_{measured} - (\beta_{hkl})^2_{instrumental}\right]^{1/2} \quad (6)$$

Where β_{hkl} are the FWHM of the diffraction peaks, $(\beta_{hkl})_{instrumental}$ found from measuring the broadening of a standard single crystal. The crystallite size broadening can be found from Scherrer formula

$$\beta_{size} = \frac{k\lambda}{D\cos\theta} \quad (7)$$

Where λ is the wavelength of the incident x-ray, k is the shape factor, D is the average crystallite size, and θ is Bragg's angle. The broadening from the strain is given by

$$\beta_{strain} = 4\epsilon\tan\theta \quad (8)$$

Where ε in the formula is the strain. If the contribution of crystallite size and strain to line broadening is independent of each other, then the total FWHM of the peak is

$$\beta_{hkl} = \frac{k\lambda}{D\cos\theta} + 4\epsilon\tan\theta \quad (9)$$

And from the above equation, W-H equation can be written as

$$\beta_{hkl}\cos\theta = \frac{k\lambda}{D} + 4\epsilon\,\mathrm{Sin}\,\theta \quad (10)$$

After the plotting of plot $\beta_{hkl}\cos\theta/\lambda$ vs. $4\sin\theta/\lambda$ plot The crystallite size and lattice strain can be determined from the slope and intercept of the linear fit plot.[106]

The X-Ray diffraction instrument used in this thesis is XRD; PANalytical EMPYREAN X-Ray diffraction instrument which has tube current equal to 40 mA and voltage equal to 45 kV.

2.2. Raman spectroscopy

Raman spectroscopy is considered as a non-destructive technique that provides a valuable information about a material's atomic structure and composition through the analysis of the shift of the incident photon caused by phonon coupling. Raman scattering occurs from the inelastic scattering of monochromatic laser beam due to the interaction with the molecular vibrations and produces a scattered light. The scattered light will have energy different from the energy of the incident light and this shift in energy will give information about the vibrational modes in the system as shown in figure 16.

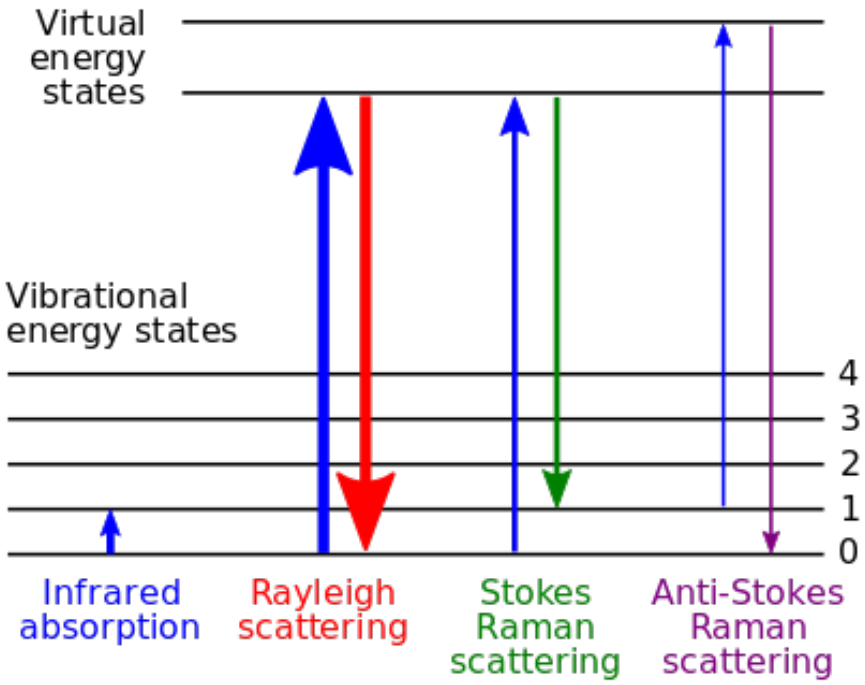

Figure 16: A schematic shows the principle of Raman spectroscopy

In Raman analysis the sample is focused with a laser beam which leads to produce an electromagnetic radiation. These radiations is then collected by a lens and sent to a monochromator. The elastic scattered radiation with a wavelength corresponds to the laser line is then filtered out by a notch filter, edge pass filter or a band pass filter. The rest of the light is detected by a detector device.

The Raman setup used in this work is Thermo Scientific Dispersive Raman Microscope

(DXR) with 532 nm laser beam shown in figure 17.

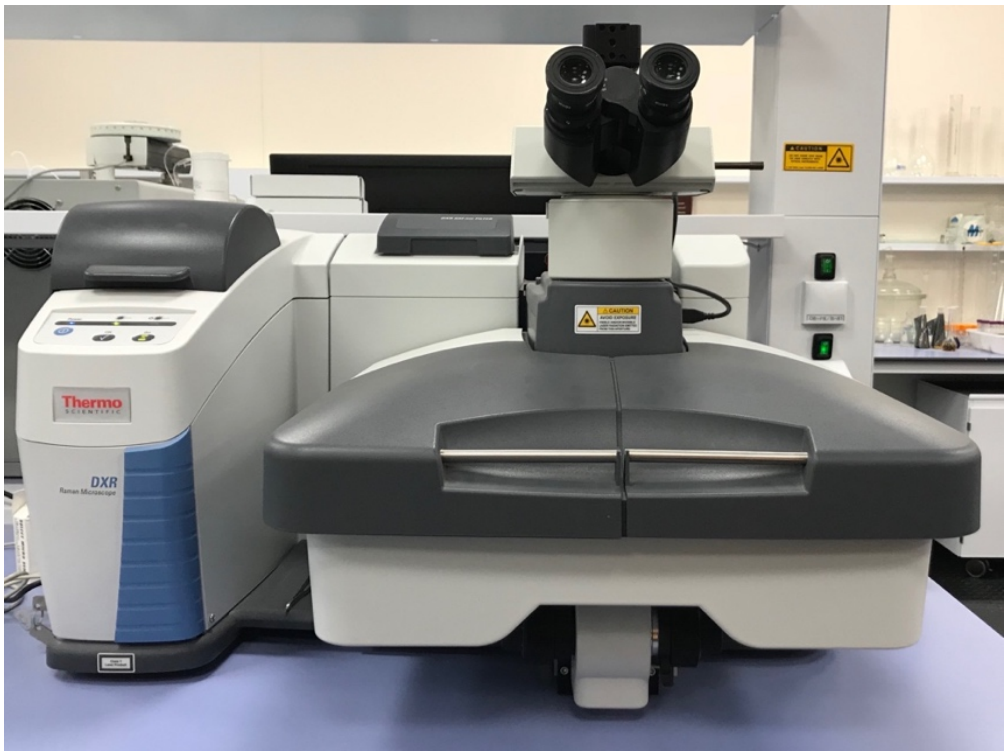

Figure 17: Raman spectroscopy device.

2.3.X-ray Photoelectron Spectroscopy (XPS)

XPS is considered as a non-destructive technique.. This technique gives information about the surface elements, and it is considered as a quantitative analysis of the surface.[107]

Figure 18 shows the principle behind this technique where an X-ray is used to knock out the electrons from their atomic orbitals at the sample surface. This phenomenon called photoelectric effect. The knocked out electrons are detected via a spectrometer where it measures the intensity of the photoelectrons as a function of binding energy. [108]

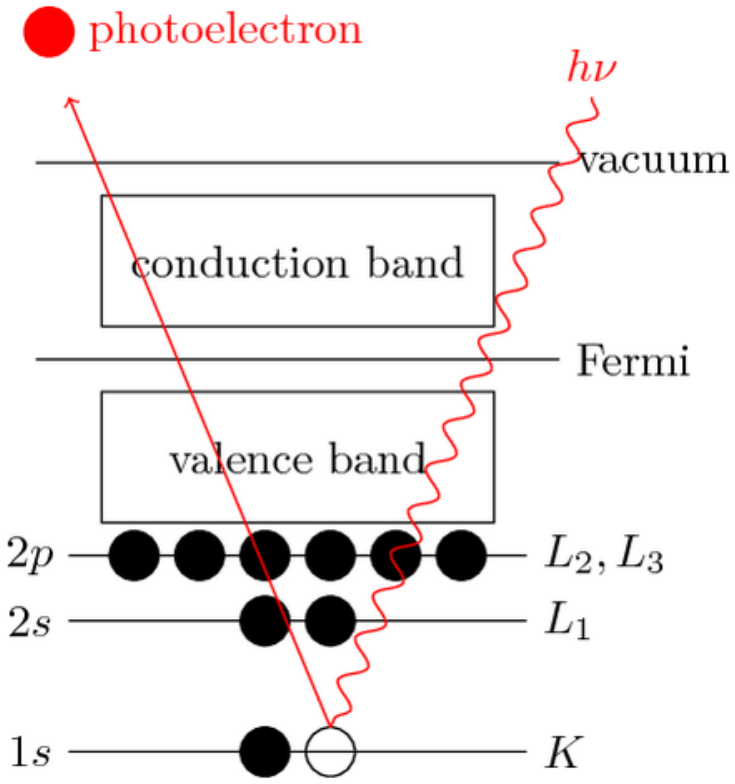

Figure 18: Schematic of photoelectric process at electron energy levels.

Figure 19 shows a typical schematic of XPS device. The photo-ejected electrons are inelastically scattered through the sample, while the other electrons undergo prompt emission with no energy loss while leaving the surface into the surrounding vacuum. The kinetic energy of the ejected electrons will be found by an electron analyzer when they present in the vacuum. Finally, an energy spectrum will be generated.

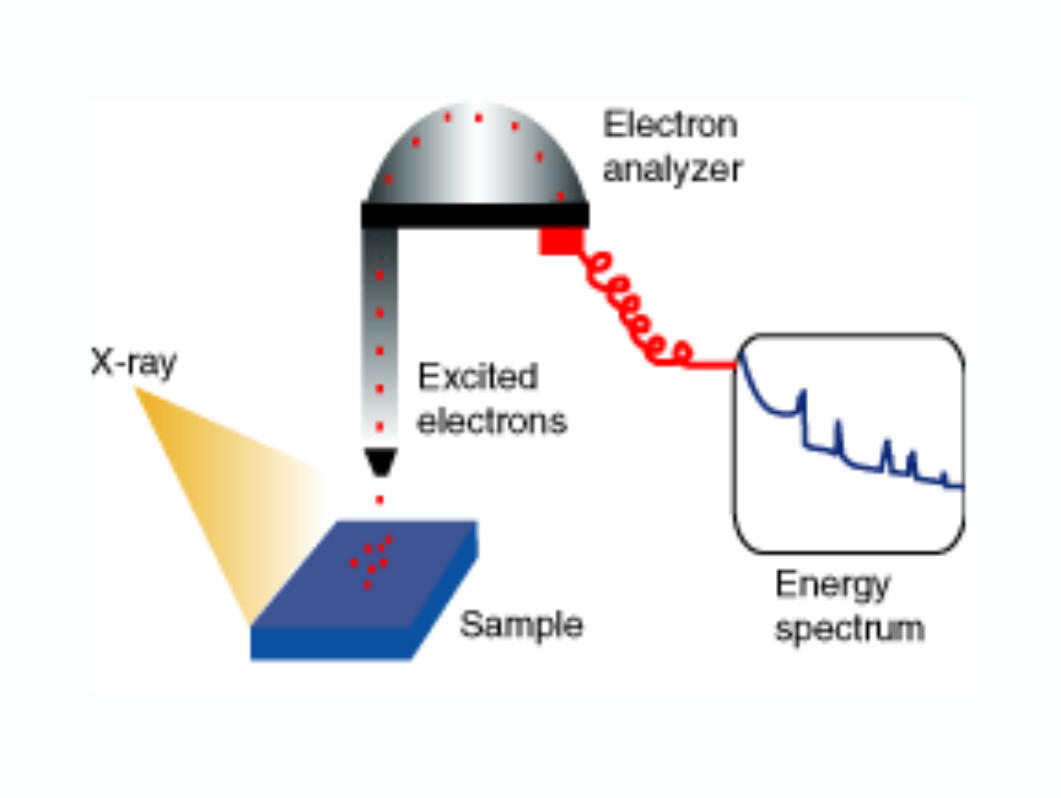

Figure 19: A schematic of XPS working principle.

This analysis technique was performed using X-ray photoelectron spectroscopy (AXIS Ultra DLD (XPS) including (SAM, ISS, MS &UPS)).

2.4. Scanning electron microscopy (SEM)

The surface morphology and topography of a film can be analyzed using SEM. The functionality of optical and electron microscopes is similar, but the difference is using electron beam instead of light. SEM has a higher resolution in the nanometer range and a smaller wavelength.[109]

The SEM principle is based on electron beam generated at the electron gun by a filament and accelerated to an anode. Then the electrons are focused with magnetic or electrostatic lenses and scanned over the sample surface. The electron beam will interact with the surface atoms differently according to the chemical composition and the morphology of the sample. Figure 20 shows the variety of signals which are possible to produces as a result of the interaction between the electron and matter. Finally, the produced backscattered or secondary electrons are collected by a detectors and a picture is formed.[108]

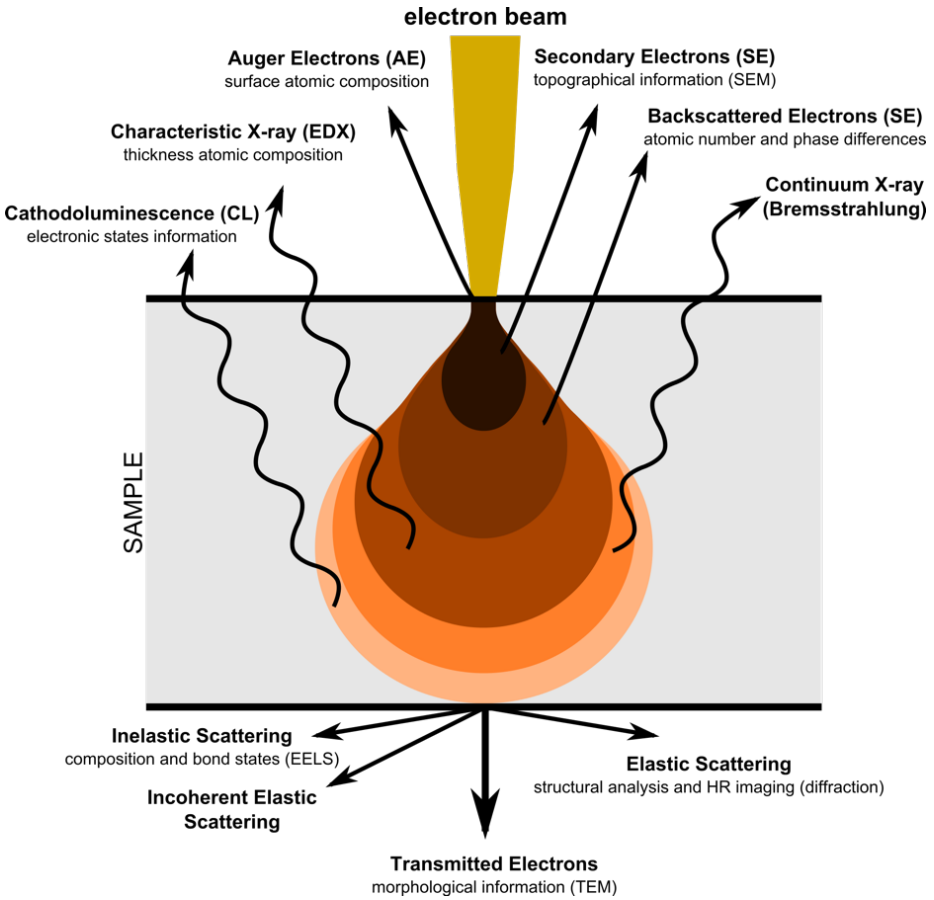

Figure 20: Types of electrons produced by an electron beam.

The surface morphology of the samples were determined using (SEM, Nova NanoSEM 450) instrument.

2.5. Energy Dispersive X-ray Spectroscopy (EDS/EDX)

EDX is an important tool to define the elemental content of a sample and it is based on the unique electromagnetic emission spectrum for each element. Electrons or X-rays are focus on the sample and excite an electron in inner shell to create an electron hole. The difference between the higher and lower energy shells released in the form of an X-ray. The principle of EDX is shown in figure 21. The amount of energy and emitted X-rays can be measured using a specific detector. [110-112]

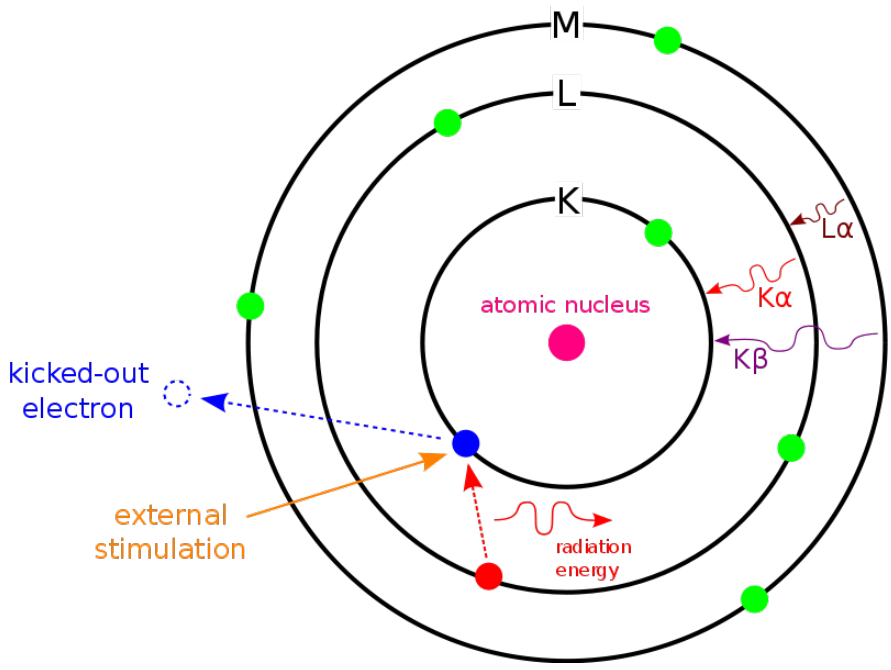

Figure 21: Schematic diagram shows the principle of EDS.

2.6. Photoluminescence (PL) spectroscopy

PL is one of the characterization techniques used in the mesurments of the optical properties of the materials. It is classified as a nondestructive technique and its used in a wide range of research applications such as photovoltaic materials.

It is based on the capability of a material to absorb a photon and re-emitting other lower energy photons. When a valance electron exited to the conduction band a hole will be created in the valance band. Once the excited electron moves to a lower energy level and recombines with the hole, a photon will be emitted as represented in figure 22. In the energy conversion principle the characteristic photon (hv = Eg) represent the band gap of the material where ($\Delta E = E_g = E_c - E_v$).[113]

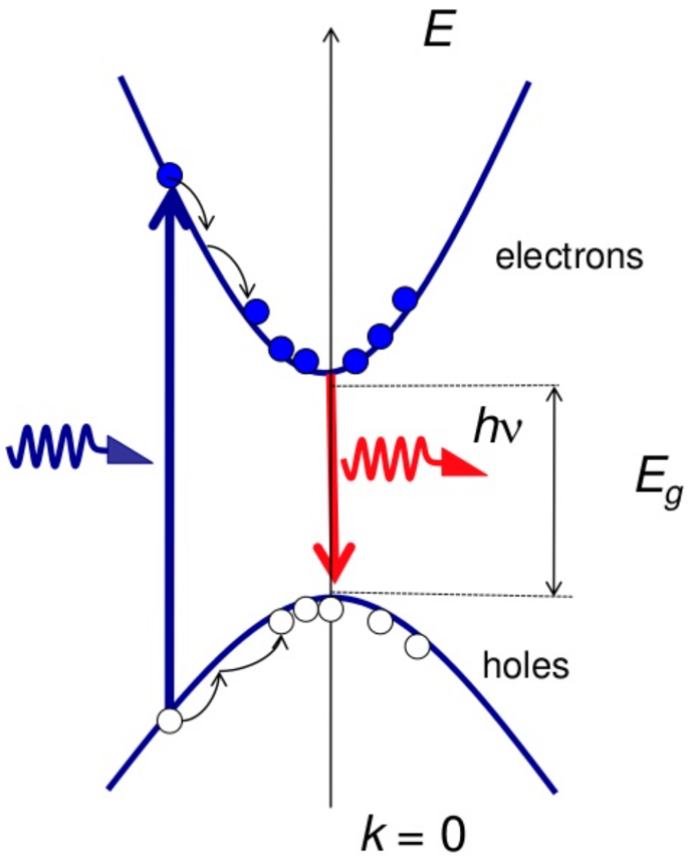

Figure 22: Energy diagram of PL process.

The device consists of a laser source, sample stage, monochromator to controls the wavelength and a detector. The PL measurements were done using Dong Woo Maple II system. The laser source wavelength used in this thesis is 532 nm shows in figure 23.

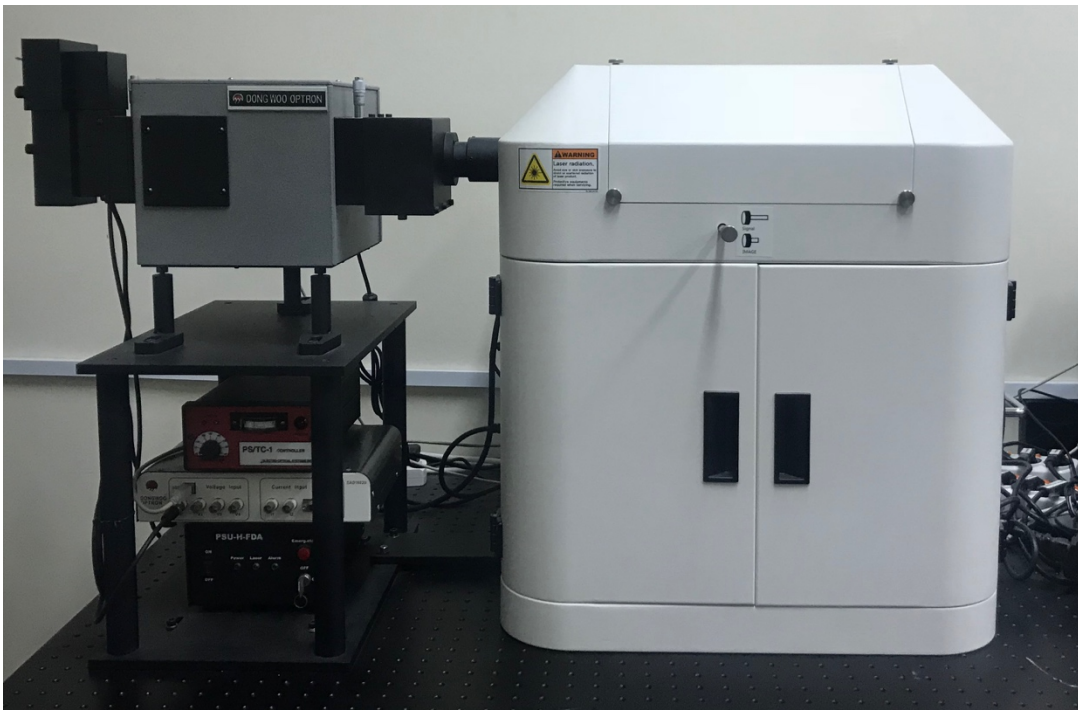

Figure 23: Photoluminescence *(PL)* spectroscopy *device.*

2.7. UV-visible spectroscopy

UV-visible spectroscopy is an analytical technique used for the quantitative determination of different substances. The electromagnetic spectrum is shown in figure 24 where the visible region is from 400 to 800 nm, while the ultraviolet region is ranging from 200 to 400 nm.

In the UV-visible spectroscopy, a beam of light is separated to its component wavelengths by diffraction grating or a prism. The monochromatic beam is split by half-mirrored into identical intensity beams. One beam passes through the reference sample,

while the other beam passes through the sample to be studied. The intensities of these light beams are then measured by a detector and the results are compared. [114]

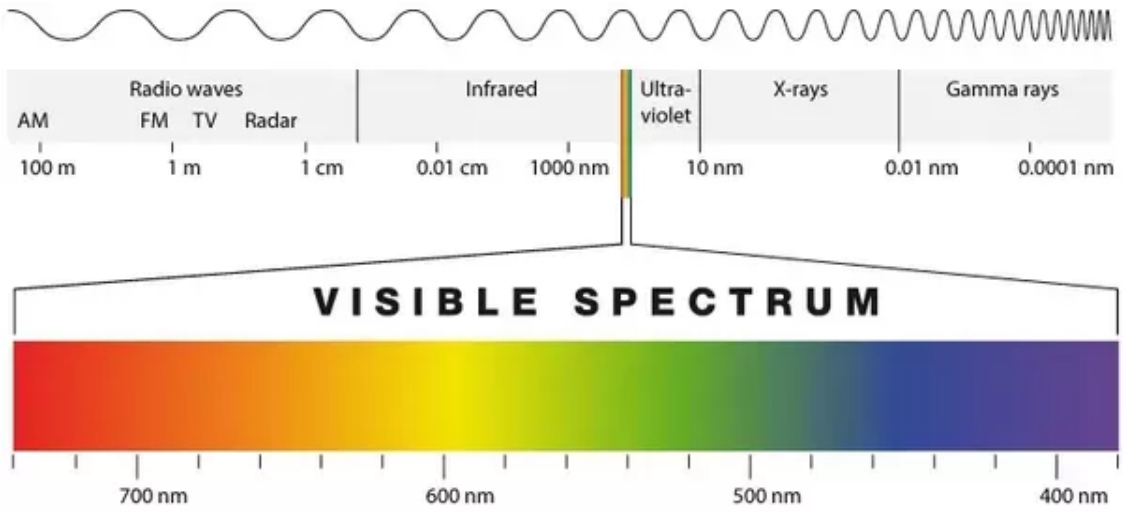

Figure 24: Electromagnetic spectrum.

The band gap can be calculated from the absorption spectra. For allowed transition in a material, the absorption coefficient near the band edge can be represented as:

$$\alpha = \frac{k(h\upsilon - E_g)^p}{h\upsilon} \qquad (11)$$

where hν is the photon energy, E_g is the band gap, p is ½ for the direct allowed transition and 3/2 for the indirect allowed transition, and k is a constant given by

$$k = \frac{e^2}{\pi n c m_e^* h^2}(2m_r)^{3/2} \qquad (12)$$

Where m_e^* and m_r are effective and reduced mass of charge carriers. Therefore, the graph of $(\alpha h\nu)^2$ vs $h\nu$ is linear near the band edge for direct band gap materials. The band gap can be calculated using the slope and the intercept of the linear part of the graph. The absorption coefficient of the material is related to the absorbance by the equation

$$I = I_o e^{-\alpha t} \qquad (13)$$

Where I and I_o represent the intensity of the light after and before the transmission through the material, and they are related by the following equation to the absorbance

$$A = \log\left(\frac{I_0}{I}\right). \qquad (14)$$

CHAPTER 4: RESULT AND DISCUSSION

1. Electrodeposition of Cu_2ZnSnS_4 thin films

In this thesis, the chemicals were purchased and then used without any purification process. The single step electrodeposition of CZTS thin films was done using an electrodeposition bath consists of the CZTS precursors 0.02 mol/L Cu_2SO_4, 0.01mol/L $ZnSO_4$ and 0.02 mol/L $SnCl_2$. 0.01 mol/L Na_2SO_4 was used as a sulfur source, while 0.2 mol/L tri-sodium citrate was added to the solution as a complexing agent. The pH of the electrolyte solution was adjusted using 0.01 mol/L tartaric acid and maintained in the range of 4.0-5.0. Figure 25 shows the prepared solution in volumetric flask.

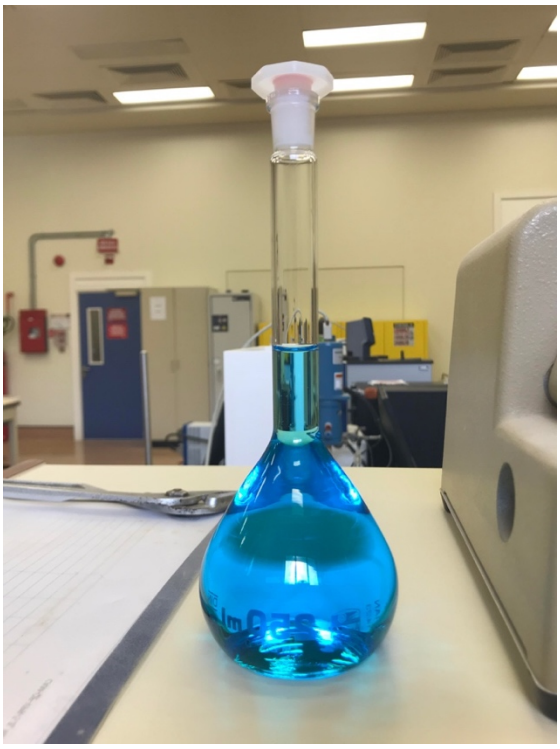

Figure 25: A volumetric flask contains the prepared solution.

Fluorine doped tin oxide (FTO) coated glass substrates with dimensions 15x20x3.2 mm are used in this work . The FTO substrates were cleaned by three steps of ultrasonication. The first step is ultrasonication using a soup solution of detergent and deionized water. The second step is ultrasonication using acetone and isopropyl alcohol, and finally the ultrasonication using deionized water. Each of these steps was done for 10 min. The electrodeposition of CZTS films was done on 15x 15 mm active area of the FTO-coated substrates. The experiments were done using a potensiostat/galvanostat Gamry

reference 3000 employing three electrode cell configurations. The films were deposited by amperometry technique using Ag/AgCl as a reference electrode, Pt as a counter electrode and FTO coated substrate as a working electrode. The substrate was immersed in the electrodeposition bath at room temperature, and at fixed potentials for 4 min. The individual electrochemical reaction of Cu-Zn-Sn-S corresponds to the following Nernst equations:[115-116]

$$Cu^{2+} + 2e^- \longrightarrow Cu \qquad E_{Cu} = 0.14\,V - \frac{RT}{2F}\ln[Cu^{2+}](vs.\,Ag\,/\,AgCl) \tag{15}$$

$$Zn^{2+} + 2e^- \longrightarrow Zn \qquad E_{Zn} = -0.96\,V - \frac{RT}{2F}\ln[\,Zn^{2+}](vs.\,Ag/AgCl) \tag{16}$$

$$Sn^{2+} + 2e^- \longrightarrow Sn \qquad E_{Sn} = -0.38\,V - \frac{RT}{2F}\ln[Sn^{2+}](vs.\,Ag\,/\,AgCl) \tag{17}$$

Where E_{Cu}, E_{Zn}, and E_{Sn} are the Nernst potentials of the metals vs. Ag/AgCl reference electrode. The concentration of ions in the electrolyte are $[Cu^{2+}]$, $[Zn^{2+}]$, and $[Sn^{2+}]$. While T is the temperature in kelvin (K), F is the faraday constant, and R is the ideal gas constant. From the above Nernst equations, the reduction potential of Cu, Zn, and Sn are 0.14 V, -0.96 V, and -0.38 V, respectively.[117-119] There are very large differences in their standard potentials, therefore it's hard to electrodeposit the CZTS precursor from a single electrolytic solution. Tri-sodium citrate was added to the electrodeposition bath in order to narrow the potential gap between the metals .[64, 120-123]

Figure 26 shows the cyclic voltammetry curve which was performed in a potential window range from 0 V to -2 V with respect to the reference electrode Ag/AgCl. From the plotted curve, a reduction peak is shown at around -1V (vs. Ag/AgCl). So, a

minimum -1 V potential was chosen for the chronoamperometric deposition of CZTS films. Since the electrolyte solution contains several reduction species with different reduction potentials. Therefore, the assignment of the reduction potential is a very important task.

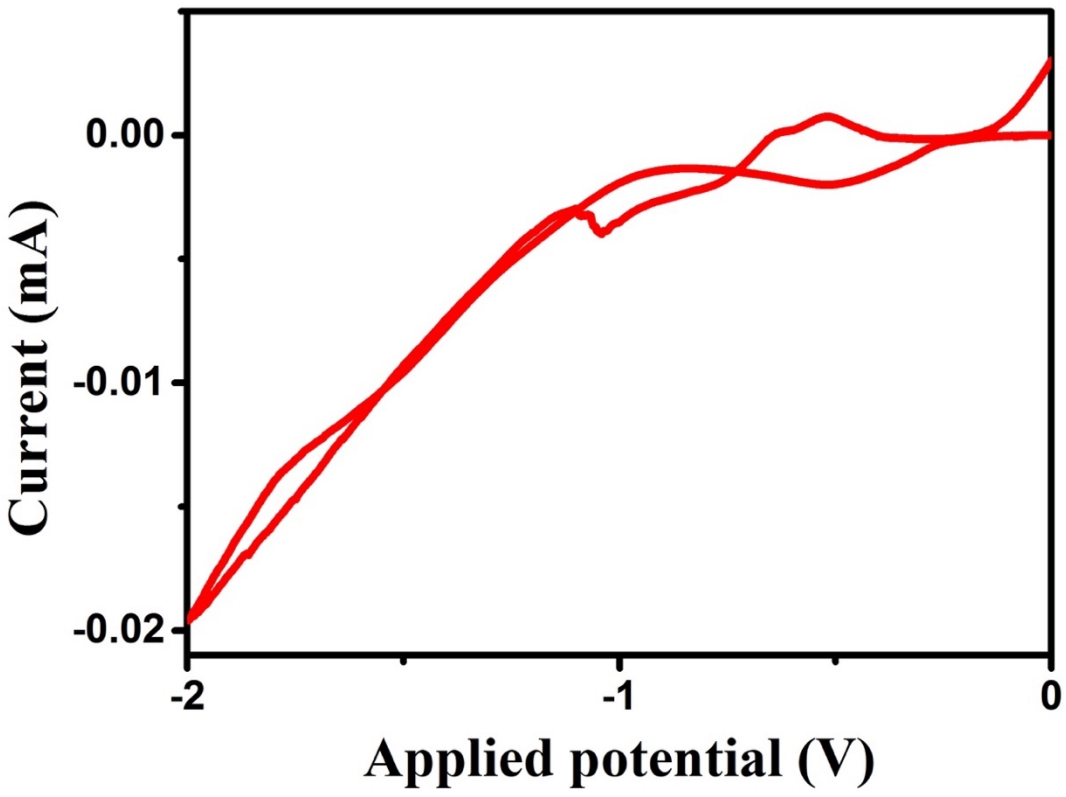

Figure 26: Cyclic Voltammetry curve of CZTS electrolyte with 10 mV/s scan rate.

After the deposition of the films they were washed with deionized water and dried at room temperature. The sulfurization process was accomplished in tubular furnace with continuous argon flow at 550 °C for 30 minutes. Sulfur powder was used in the sulfurization process and it was loaded into a quartz tube. The excess sulfur powder was removed after the sulfurization by the dipping of the films in isopropyl alcohol. The furnace used in this work is (GSL 1500X-OTF) and the device is shown in figure 27.

Figure 27: The tube furnace used in the sulfurization process.

2. Effect of deposition potential on the prosperities of CZTS thin films.

The effect of the deposition potential is studied in this chapter. We investigated the effect of deposition potential on the structural, compositional and morphological properties on CZTS thin film. The electrodeposition of these films was performed at fixed potentials of -1.10 V, -1.20 V, -1.25 V, -1.30 V, and -1.35 V.

2.1.Structural properties

The XRD measurements were performed using PANalytical diffractometer, a copper anode was used to generate the X-rays. The $K\alpha$ wavelength is 1.54 A°, and the scans were done with 45 kV, a current of 40 mA, a step size of 0.0131 and the scan speed was 37.995 s/ °. The 2θ scan ranged from 20° to 80° for all samples. XRD analysis was done in order to investigate the formation of CZTS kesterite phase after sulfurization. Figure 28 shows the XRD of the sulfurized CZTS samples which were deposited at different potentials. The figure shows that the major characteristic peaks of the kesterite phase of CZTS were found in all deposited samples, which can be indexed as (112), (200), (220), and (312) planes. These peaks are also correlate well with the ICCD values of CZTS kesterite phase (ICDD Ref. No: 00-026-0575). [66] The peaks at 2θ = 26.56°, 33.77°, 37.81°, 42.78°, 51.64°, 61.74°, and 65.77° represent the XRD peaks of the FTO substrate and match well with the (JCPDS 46-1088).

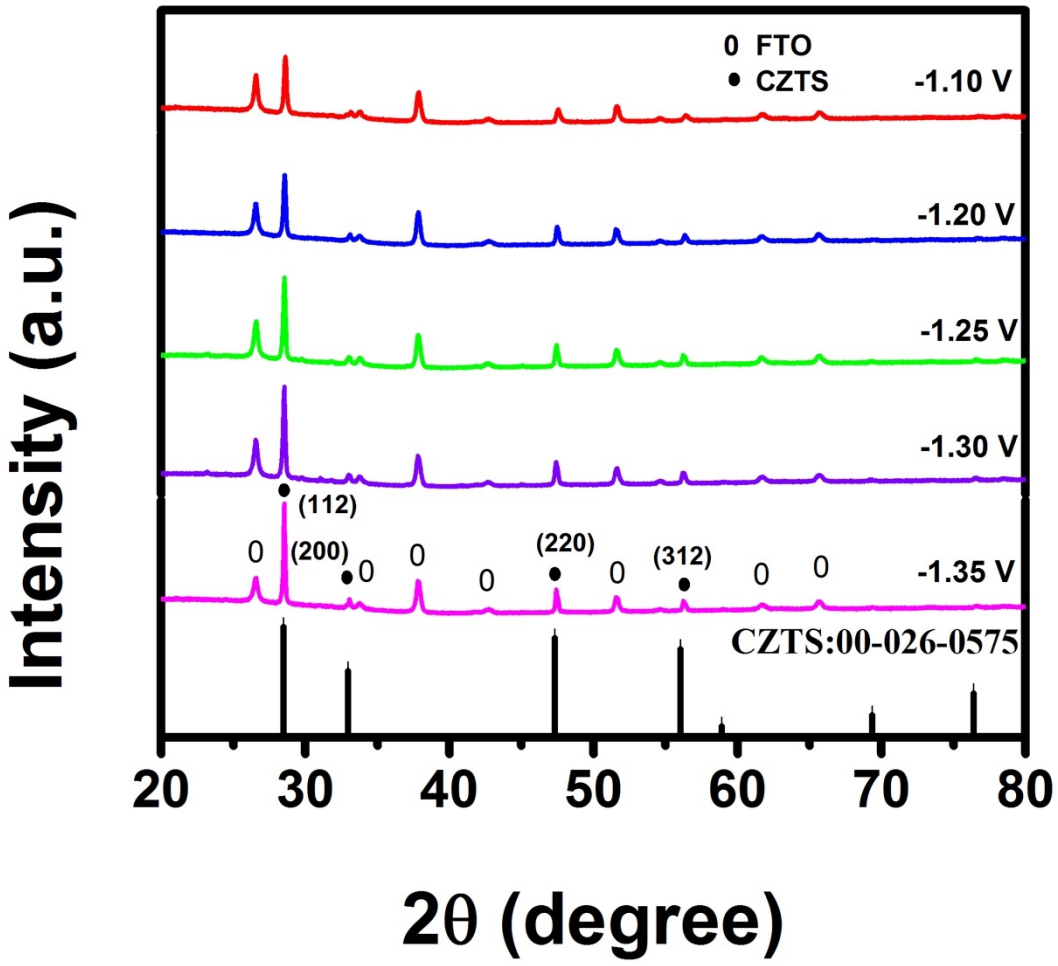

Figure 28 : XRD analysis of the CZTS thin films deposited at different deposition potentials.

The growth orientations and the lattice parameters of the CZTS thin films deposited at different potentials were calculated using the XRD data and Scherrer formula and listed in table 1.

Table 1: The calculations of the lattice parameters from (112) and (220) XRD peaks of CZTS thin films deposited at different potentials.

Deposition potential (V)	Peak Position (degree)	Index of plane	Inter planar distance (A)	FWHM of (112) plane (degree)	Lattice Parameters (A)	Crystallite size (nm)
-1.10	28.62	(112)	3.115	0.18	a = 5.400	45.53
	47.57	(220)	1.909		c = 10.77	
-1.20	28.57	(112)	3.120	0.175	a = 5.411	46.82
	47.46	(220)	1.913		c = 10.78	
-1.25	28.54	(112)	3.123	0.169	a = 5.414	48.48
	47.44	(220)	1.914		c = 10.80	
-1.30	28.53	(112)	3.124	0.165	a = 5.418	49.659
	47.4	(220)	1.915		c = 10.80	
-1.35	28.53	(112)	3.124	0.157	a = 5.417	52.19
	47.41	(220)	1.915		c = 10.80	

It is clear that there is a variation in the full width at half maximum (FWHM), the intensity of the (112) plane, and the crystallite size among the samples with different deposition potentials. As the potential varied from -1.1 to -1.35, the FWHM of the (112) plane decreases and the intensity increases indicating the enchancment of the crystalline quality of the films with increasing the negative potential. In addition to that, the crystallite size increases with increasing the negative potential. We could not increase the negative potential further because of the peel off of the films after -1.35 V potential.

The tetragonal Cu_2SnS_3 and cubic ZnS are possible secondary phases and have similar XRD peak positions and lattice parameters as CZTS crystal structure. Consequently, it is very difficult to differentiate these phases using the XRD technique, therefore the actual CZTS kesterite phase is verified by Raman spectroscopy. These secondary phases have different Raman shifts compared to CZTS Raman shifts.

Figure 29 represents the Raman spectra of all sulfurized CZTS thin films deposited at different potentials. The major peaks of CZTS are located at 288 cm^{-1}, 338 cm^{-1}, and 368 cm^{-1}.[64] These peaks were found in the samples deposited at -1.30 V and -1.35 V which confirm the presence of CZTS kesterite phase. The peak at 338 cm^{-1} was the highest in the intensity while the other two peaks appeared with low intensity. These peaks correspond to A_1 phonon mode of CZTS kesterite phase.[120] The samples deposited at -1.1 V, -1.2 V, and -1.25 V exhibit peaks around 294-299 which corresponds to tetragonal Cu_2SnS_3.[121] The presence of this secondary phase is correlated with the EDS results that show a poor zinc films stoichiometry. The intensity of the peak at 338 cm^{-1} is highest for the sample deposited at -1.35 V; which indicates an improved crystallinity of the sample.

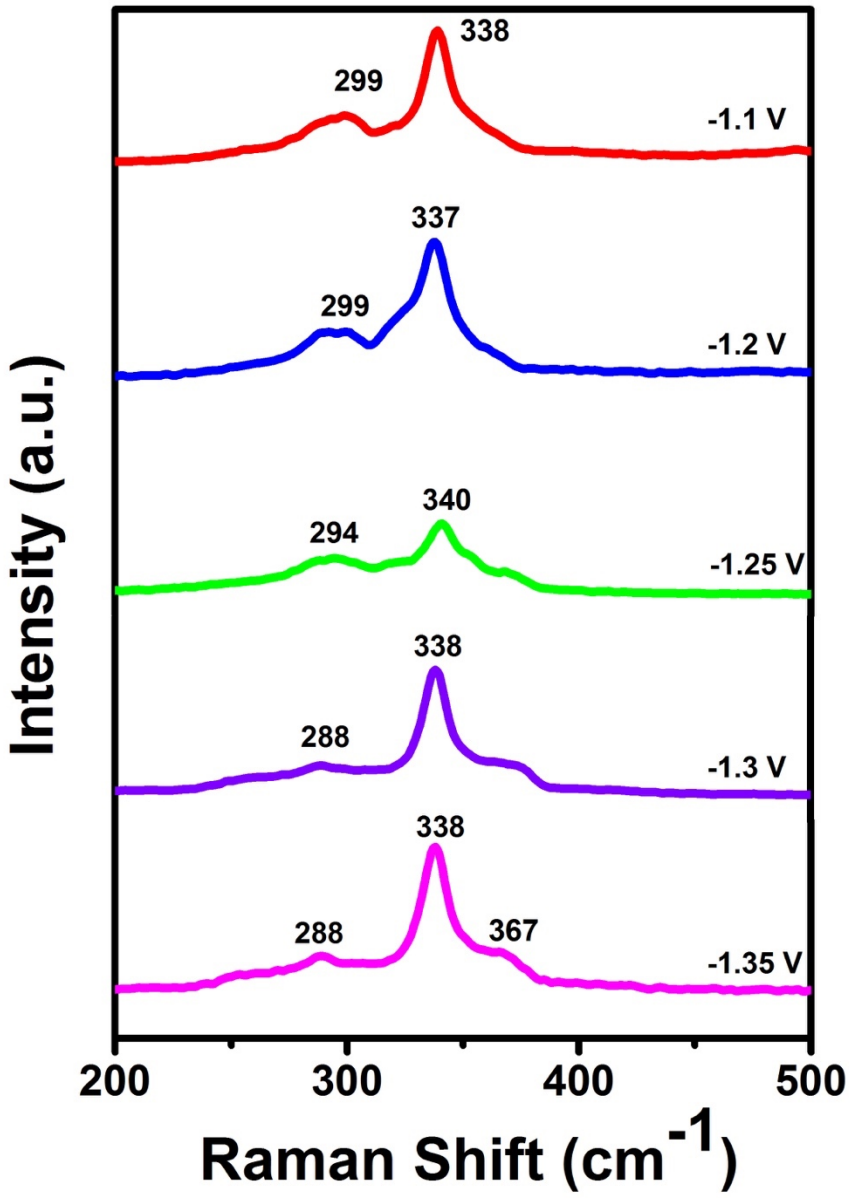

Figure 29: Raman analysis of CZTS thin films deposited at different potentials.

2.2.Compositional and morphological analysis

The XPS measurements were performed in order to classify the elemental composition of the CZTS thin films. The XPS analysis of Cu 2p, Zn 2p, Sn 3d, and S 2p were performed. The peaks separation gives information about the state of the metals. Figure 30 shows the XPS spectra of Cu 2p for all CZTS samples deposited at different potentials, the separation between the Cu $2p_{3/2}$ and Cu $2p_{1/2}$ ranges between 19.8 and 19.9 eV in all CZTS samples ,which is in good agreement with the standard separation (19.9 eV) of Cu (+1) state.[124] Figure 31 shows the XPS spectra of Zn 2p. The peak separation of about 23 eV between Zn $2p_{3/2}$ and Zn $2p_{1/2}$ indicates the presence of Zn(+2) state. Figure 32 shows the XPS spectra of Sn 3d . Peak separation ranges between 8.4 and 8.5 eV, observed between Sn 3d5/2 and Sn 3d3/2, indicates the Sn (+4) state. In addition, figure 33 shows the XPS spectra of S 2p for all CZTS samples deposited at different potentials. The S 2p peaks are positioned at 161.7 and 162.9 eV, which are consistent with the binding energy of sulfur in sulfide state of CZTS.[125]

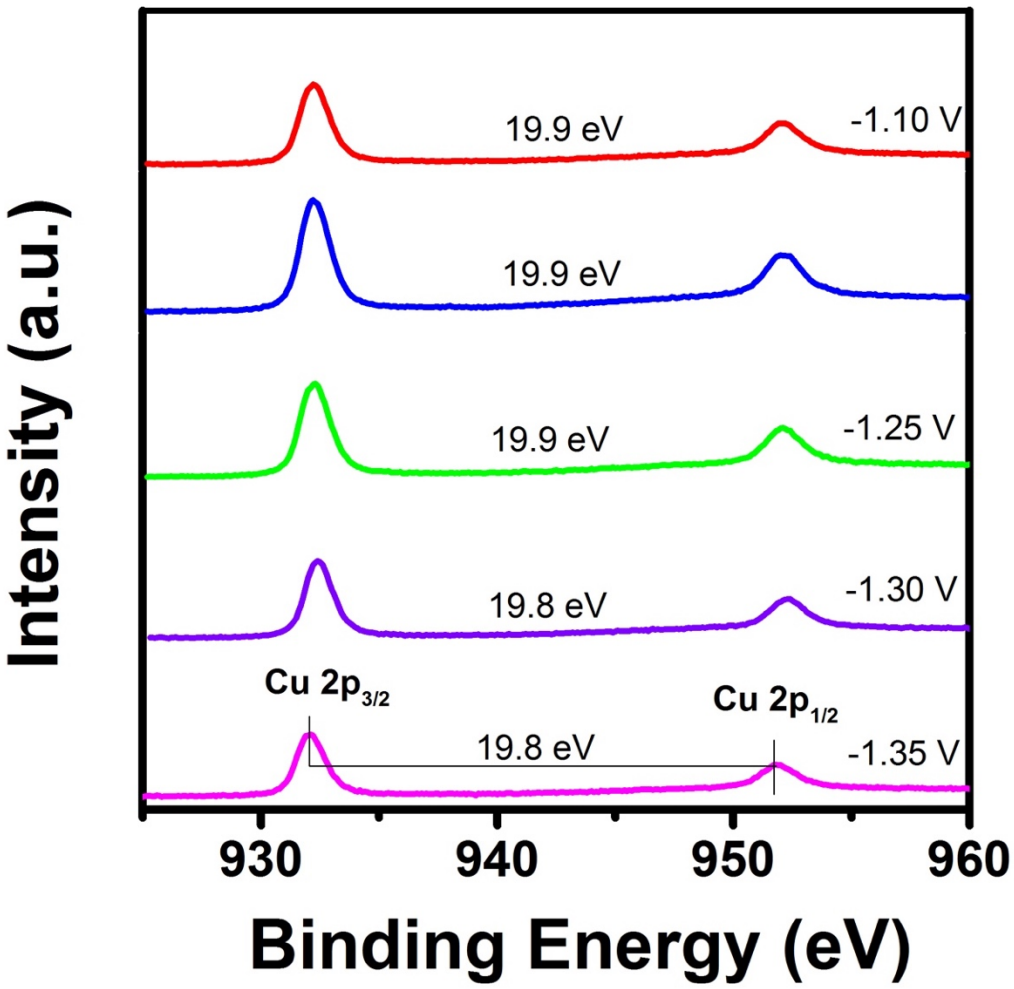

Figure 30 : XPS analysis of Cu in CZTS thin films deposited at different potentials.

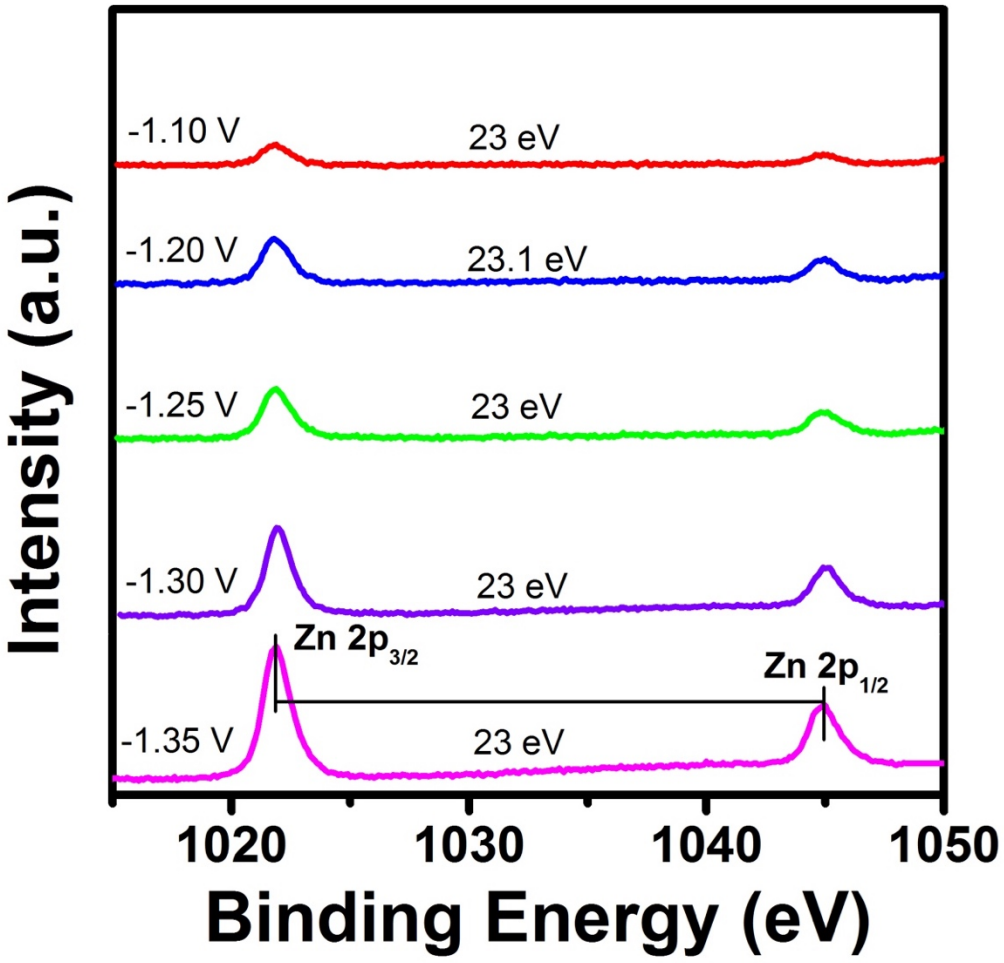

Figure 31: XPS analysis of Zn in CZTS thin films deposited at diffenet potentials .

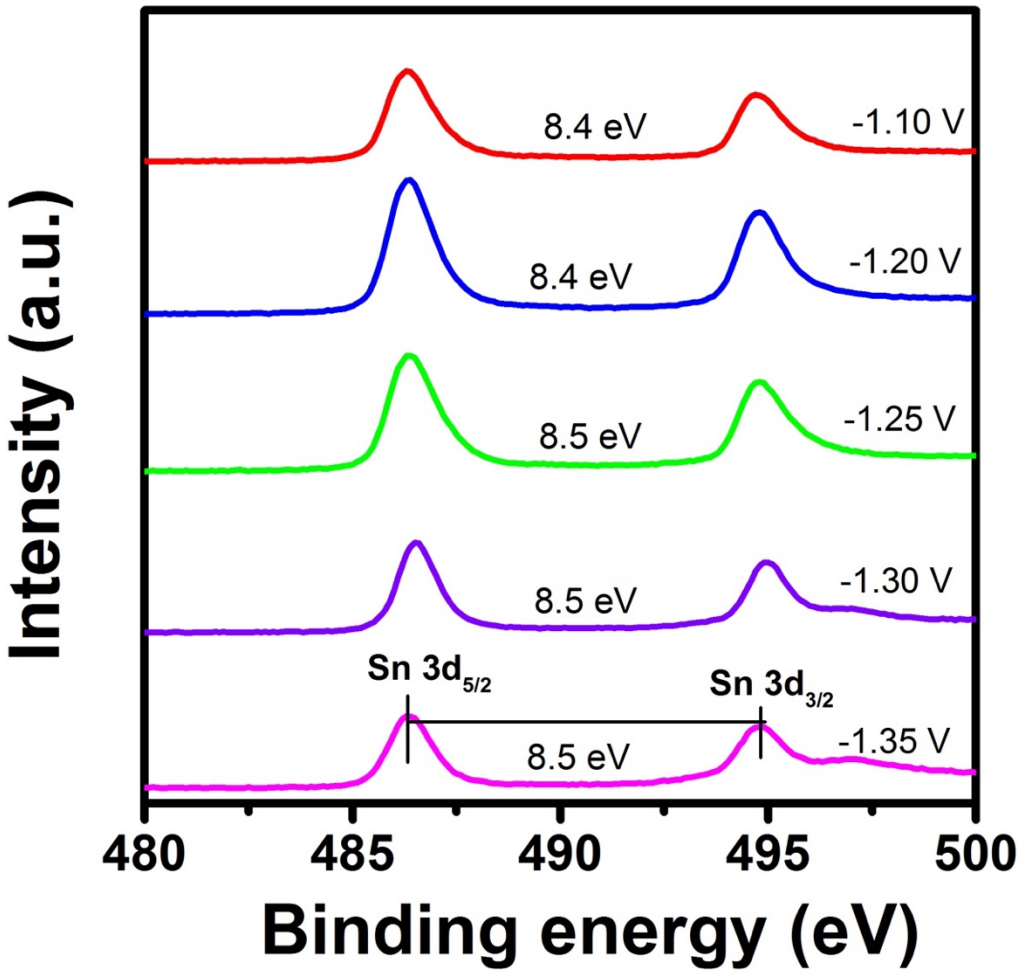

Figure 32: XPS analysis of Sn in CZTS thin films deposited at different potentials.

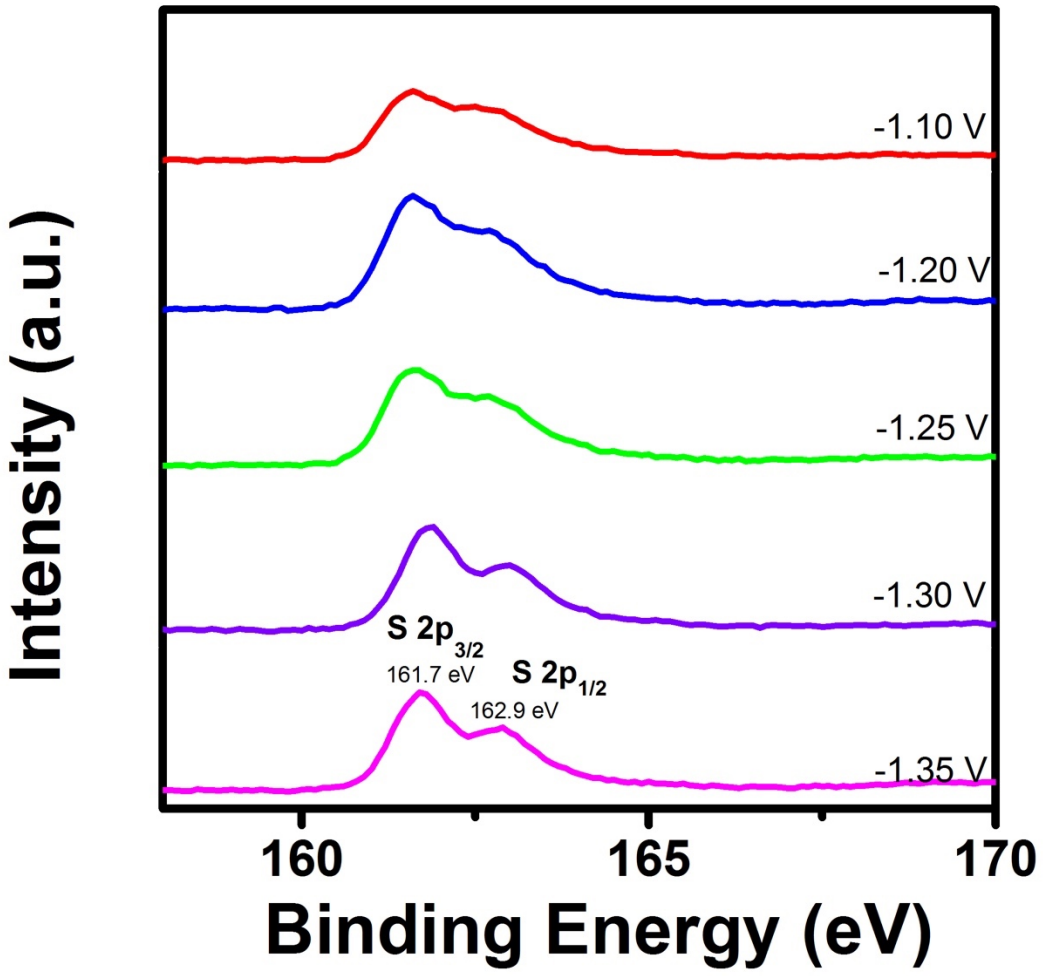

Figure 33: XPS analysis of S in CZTS thin films deposited at different potentials.

The stoichiometry of the essential elements after sulfurization was identified using EDS analysis. The ideal atomic percentage of Cu:Zn:Sn:S in the kesterite CZTS phase is 2:1:1:4 and that of the CZTS films deposited at different potentials is presented in figure 34. At potentials more positive than -1.30 V the components of the films are not deposited with appropriate stoichiometry on the FTO substrate. As the deposition potential becomes more negative, the zinc atomic percentage is increased, while the atomic percentage of copper is decreased. As shown in table 2, the best stoichiometry was achieved at -1.35 V deposition potential with the ratios of Cu / (Zn+Sn) < 0.9 and Zn / Sn > 1 which is in agreement with the literature for high absorption performance.[126] The EDS spectrum of the sample deposited at -1.35 V is shown in figure 35.

A specific reduction potential is necessary to be offered to reduce the Zn species in the electrolyte, and this will increase the Zn atomic percentage in the produced CZTS film.[123] Hence, It is clearly shown that the deposition potential affects the composition of the deposited CZTS thin films.

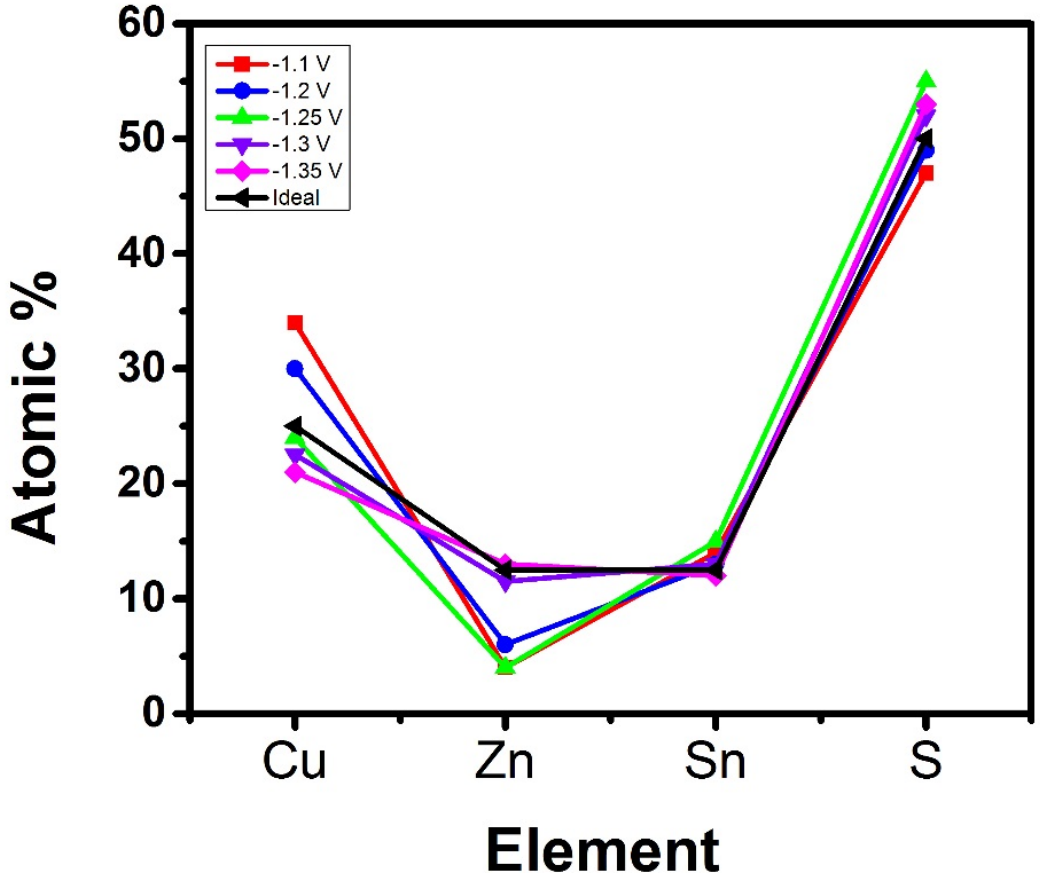

Figure 34: EDS composition plot of sulfurized CZTS samples deposited at different potentials.

Table 2: The atomic percentage of CZTS thin films deposited at different potentials.

Deposition potential	Cu	Zn	Sn	S	Cu/(Zn+Sn)	Zn/Sn
-1.10 V	34	4	14	47	1.88	0.28
-1.20 V	30	6	13	49	1.57	0.46
-1.25 V	24	4	15	55	1.26	0.26
-1.30 V	22.5	11.5	13	52	0.91	0.88
-1.35 V	21	13	12	53	0.84	1.08

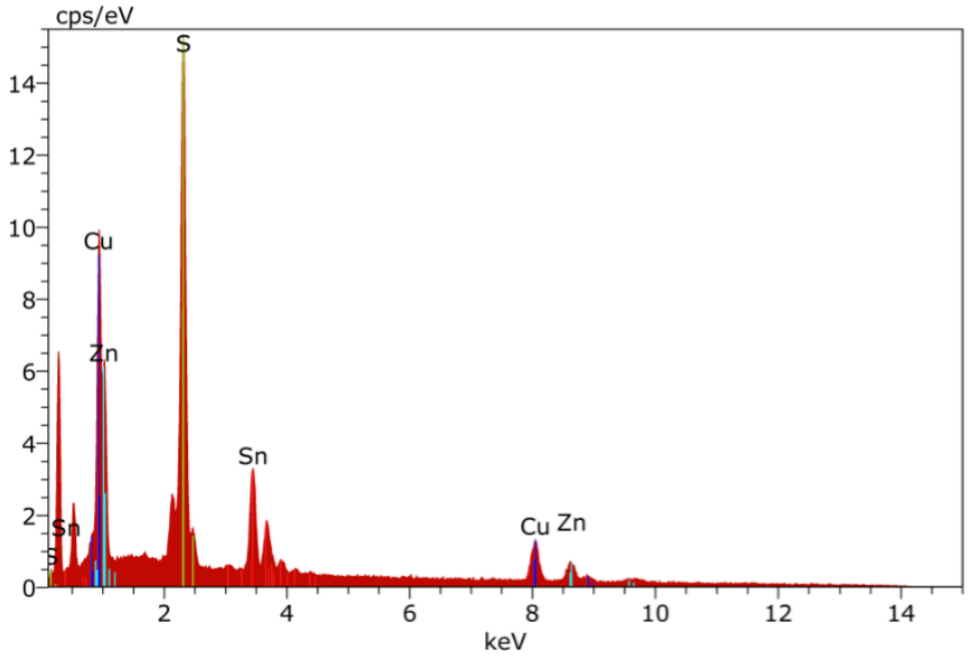

*Figure 35 :*The EDS spectrum of the CZTS sample deposited at -1.35V.

3. Effect of Sulfur amount on CZTS thin films

3.1.Introduction

The determination of the sutaible parameters to prepare a highly crystalline and pure CZTS thin film is very important task. The sulfurization process is on of these parameters which needs to be studied and optimized. There are different parameters that affect the sulfurization process such as the sulfurization time, sulfurization temperature, temperature ramping rate, and the sulfurization atmosphere. Most ofthese parameters have been studied and reported, but till now there is no study about the effect of the amount of sulfur used during sulfurization process. In this chapter, the effect of sulfur amount incorporated into the Cu-Zn-Sn precorsor throughout the sulfurization process have been studied. The ideal composition of sulfur is 50 atomic percentage for the pure kesterite phase CZTS.

A set of identical CZTS thin film samples has been deposited at -1.35 V (vs. Ag/AgCl) for 4 min. The samples were sulfurized in a quartz tube furnace under Ar atmosphere for 30 min at 550 °C. Different sulfur amounts were used (5 mg, 15 mg, 25 mg, 35 mg, and 50 mg).

3.2.Structural properties

The structural properities were investigated using XRD and Raman analysis. The XRD scans were performed to insight the surface phases of CZTS thin film after sulfurization. Figure 36 shows the XRD results of CZTS thin films sulfurized using 5, 15, 25, 35, and 50 mg of sulfur.

The highest intensity peak is located at ($2\theta = 28.50°$). Weak intensity peaks are locatedat ($2\theta = 32.90°$, 47.31°, 56.03°, 69.24°, and 76.37°). The films sulfurized using less than 35 mg sulfur, shows a low intensity of peaks, while the film sulfurized using 50 mg sulfur shows the peaks of CZTS kesterite phase along with a clear secondary phase at ($2\theta = 30.2^0$, and 31.9^0) which corresponds to SnS secondary phase and matches with the (ICDD ref. No. 00-039-0354).

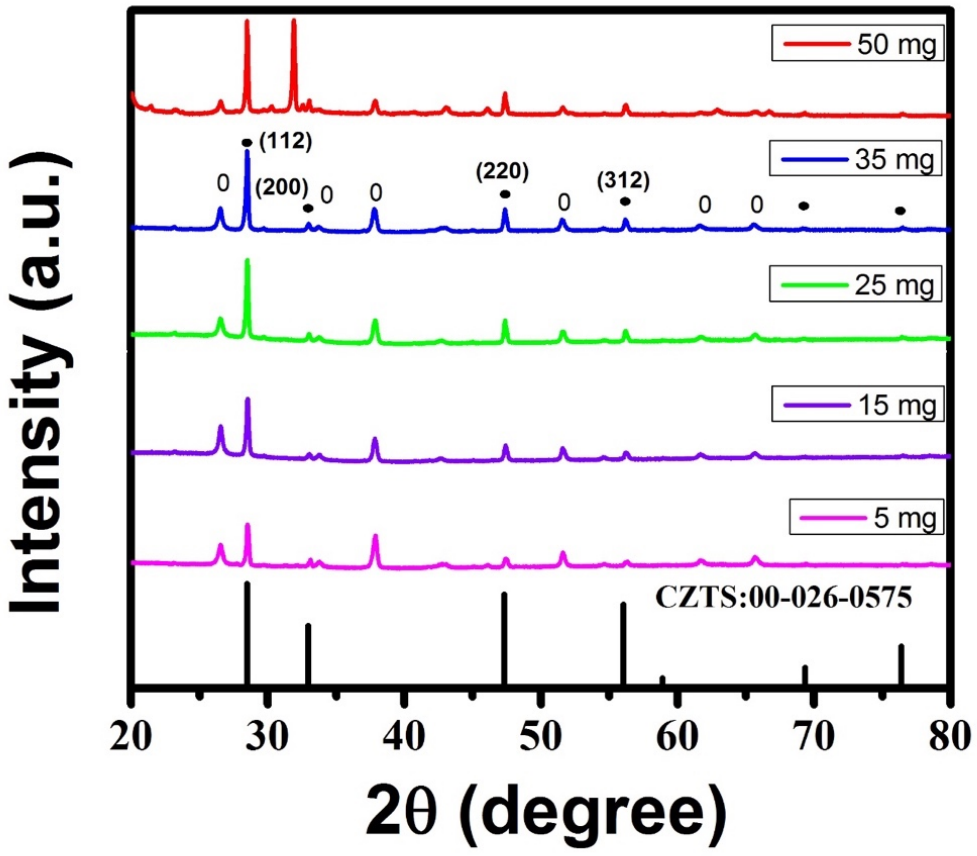

Figure 36: XRD analysis patterns of the CZTS thin films sulfurized using different amounts of sulfur as labeled.

Figure 37 shows the raman spectra of CZTS films sulfurized using diffent amounts of sufur. The film sulfurized using 35 mg of sulfur shows three peaks related to CZTS kesterite phase. The highest intensity peak was observed at 338 cm^{-1} beside two weak peaks at 288 cm^{-1} and 367cm^{-1}. The other films sulfurized using 25 mg,15 mg, and 5 mg of sulfur exhibite same peaks as 35 mg sample but with lower intensities and broader peaks.. The film sulfurized using 50 mg sulfur showed Raman peak at 239 cm^{-1} which corresponds to SnS phase and confirms the XRD results.[127] Therefore, the Raman and XRD analyses suggest that the film sulfurized using 35 mg sulfur has a better kesterite phase than the other films.

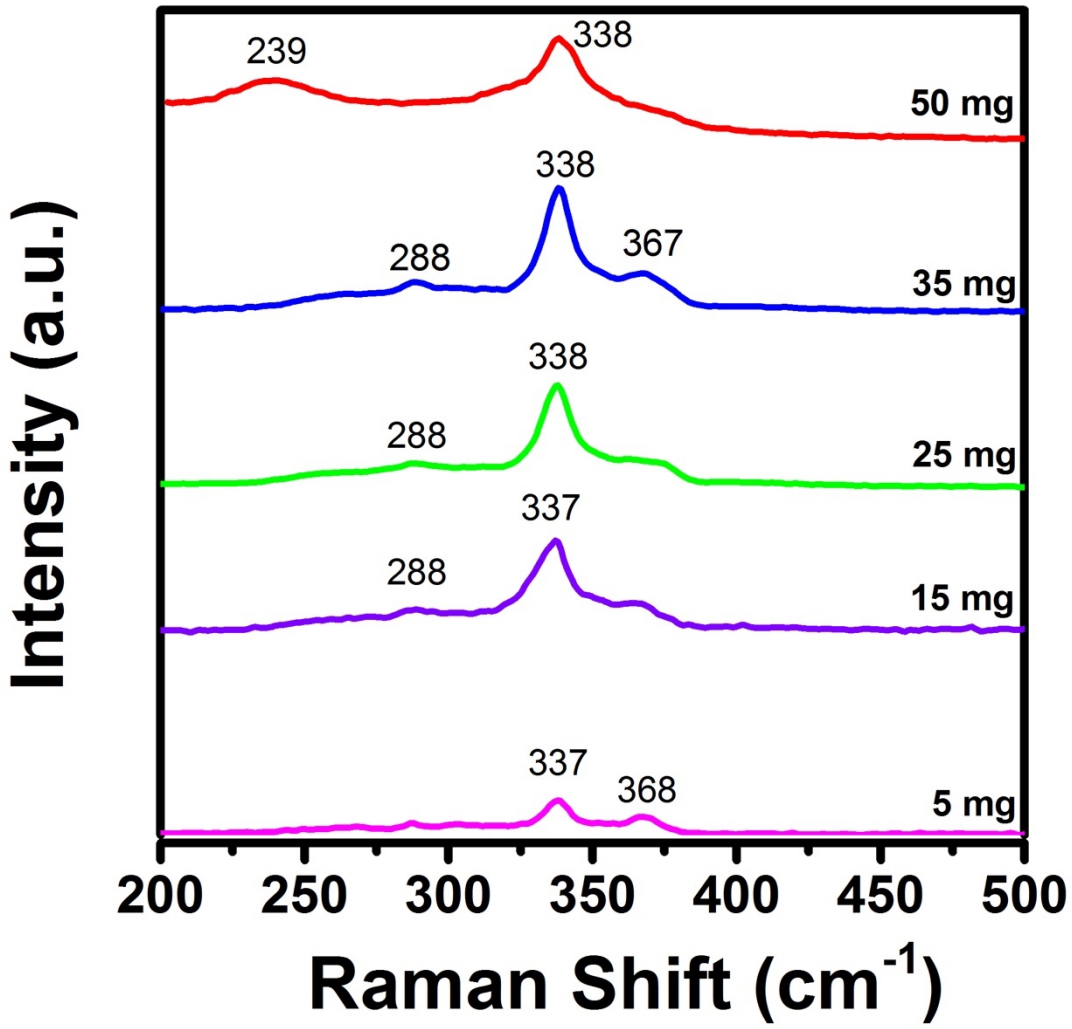

Figure 37: Raman spectra of CZTS thin films sulfurized using different amounts of sulfur as labelled.

3.3.Compositional and morphological analysis

To confirm the CZTS samples composition and to confirm that Cu, Zn, Sn, and S were presented, EDS analysis was performed. Table 3 shows the composition of CZTS thin films sulfurized using differents sulfur amounts. The atomic percentage of sulfur is between 47-54 at % after the sulfurization process, and it was increasing as the sulfur mass increases. Figure 38 shows the composition of the films. For the film sulfurized using 35 mg sulfur the stoichiometric was closer to the stoichiometry. The observation of the off-stoichiometric values in other samples indicates the existence of secondary phases along with the CZTS phase. The film sulfurized using 35 mg of sulfur showed 50 atomic percentage of sulfur and the film was Cu-poor and Zn- rich. Figure 39 shows the EDS spectrum of the CZTS film sulfurized using 35 mg sulfur.

Table 3 : The atomic percentage of Cu, Zn, Sn, and S in the CZTS thin film sulfurized using different amounts of sulfur.

Amount of Sulfur	Cu	Zn	Sn	S	Cu/(Zn+Sn)	Zn/Sn
5 mg	36.6	13.4	3	47.4	2.2	4.4
15 mg	25	16	9	49.5	1	1.7
25 mg	22	11.5	16.7	49.6	0.7	0.68
35 mg	20	13	11	50	0.83	1.1
50 mg	21	12	12	54	0.8	1

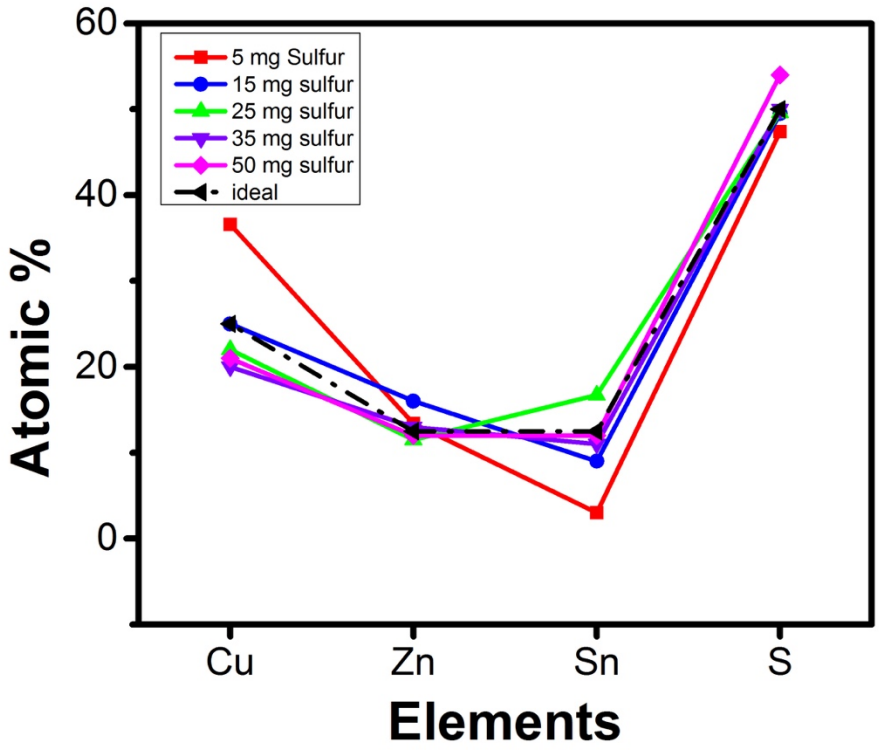

Figure 38: EDS analysis results of the CZTS films sulfurized using different amount of sulfur.

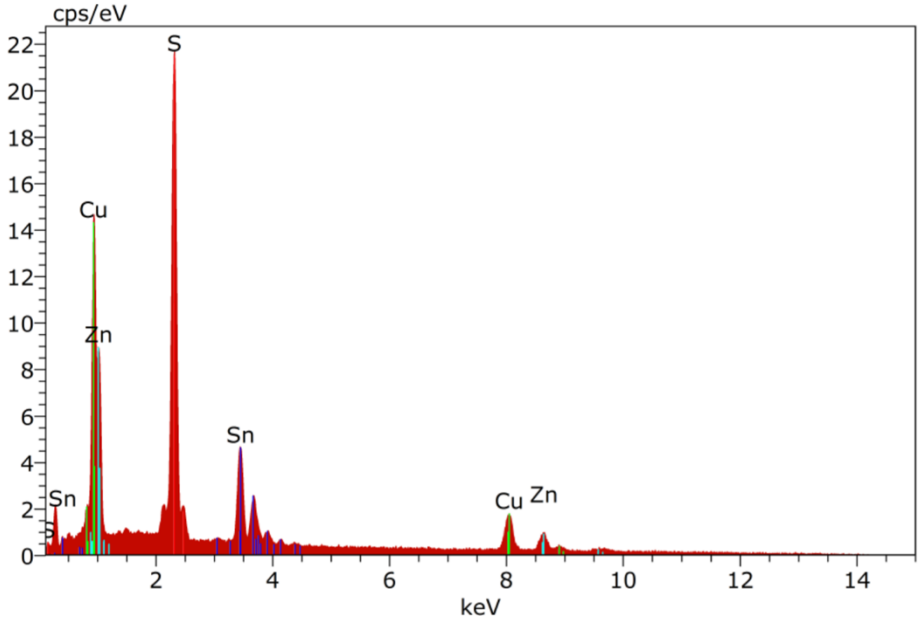

Figure 39: The EDS spectrum of CZTS sample sulfurized using 35 mg sulfur.

Cross sectional SEM image of the CZTS thin film on FTO coated glass substrate deposited using 35 mg sulfur is shown in figure 40. It shows a large grain size CZTS film. The large grain size is required for obtaining high performance solar cells. The average thickness of the CZTS film is about 1µm.

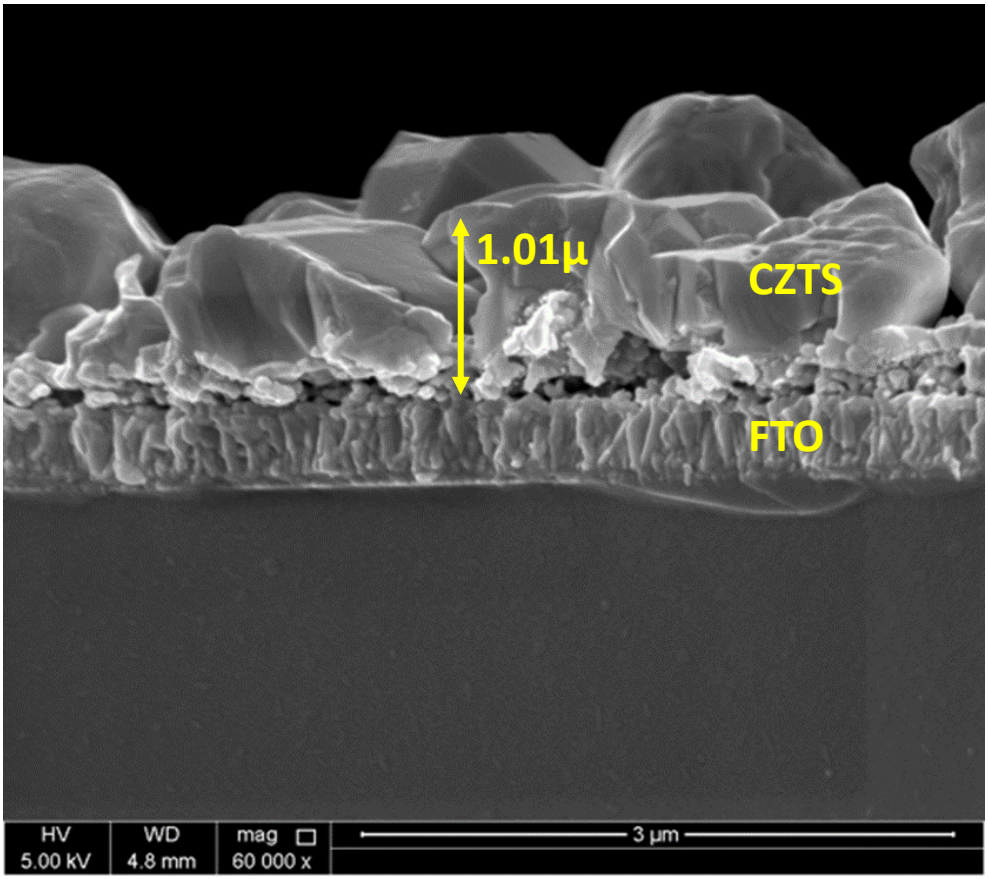

Figure 40: SEM cross section images of CZTS thin film on FTO coated glass substrate deposited using 35 mg sulfur.

The most basic requairments for a high performance of solar cells are the high absorption coefficent and an optimal band gap of 1.5 eV for CZTS absorber layer. Therefore, we used Uv-visible absorption measurments to identify the band gap and the absorption coffecient of the CZTS film. The optimal film was deposited at -1.35 V for 4 min and sulfurized using 35 mg of sulfur. This film has the best CZTS kesterite phase acccording to XRD, Raman, EDS and SEM analysis. A UV-visible spectrometer was used with a wavelength ranging from 400-1200 nm.

The UV-vis absorption spectrum absorption spectrum of the CZTS film deposited at -3.5 V and sulfurized using 35 mg sulfur is shown in figure 41. From the figure it is clear that the absorption is high in the visible region. Figure 42 shows an optical band gap of 1.5 eV. This band gap is determined by ploting $(\alpha h\nu)^2$ as a function of the photon energy ($h\nu$) and the extrapolation of the linear part of the curve to the photon energy axis. An optical band gap of 1.5 eV is determined for the CZTS thin film.[128-129] In addition, the optical absorption coefficient (α) was calculated and it was found to be 10^4 cm^{-1}.

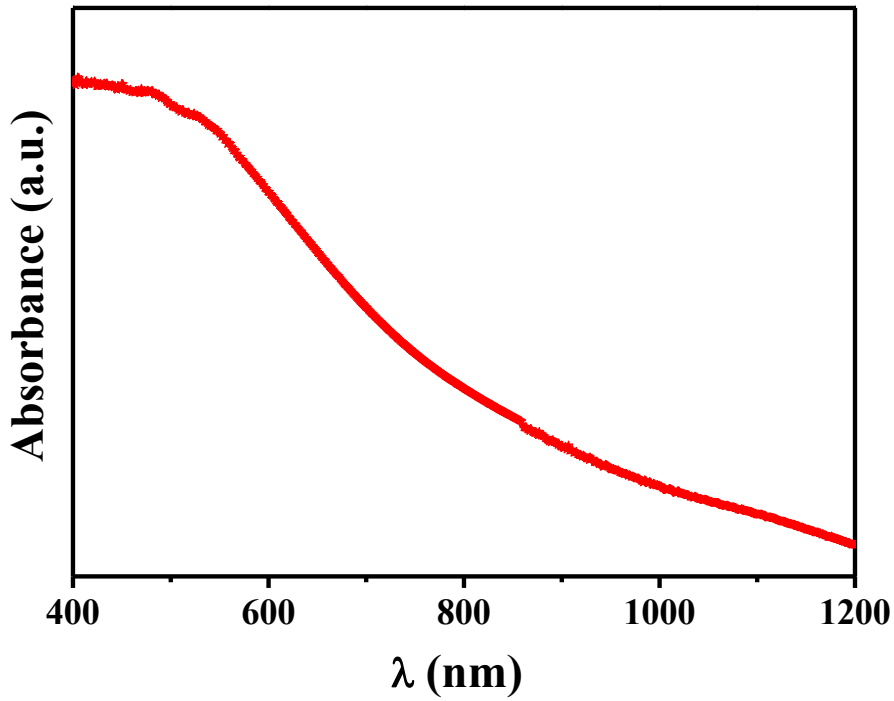

Figure 41: Absorbance spectrum of CZTS thin film deposited at -1.35V and sulfurized using 35 mg sulfur.

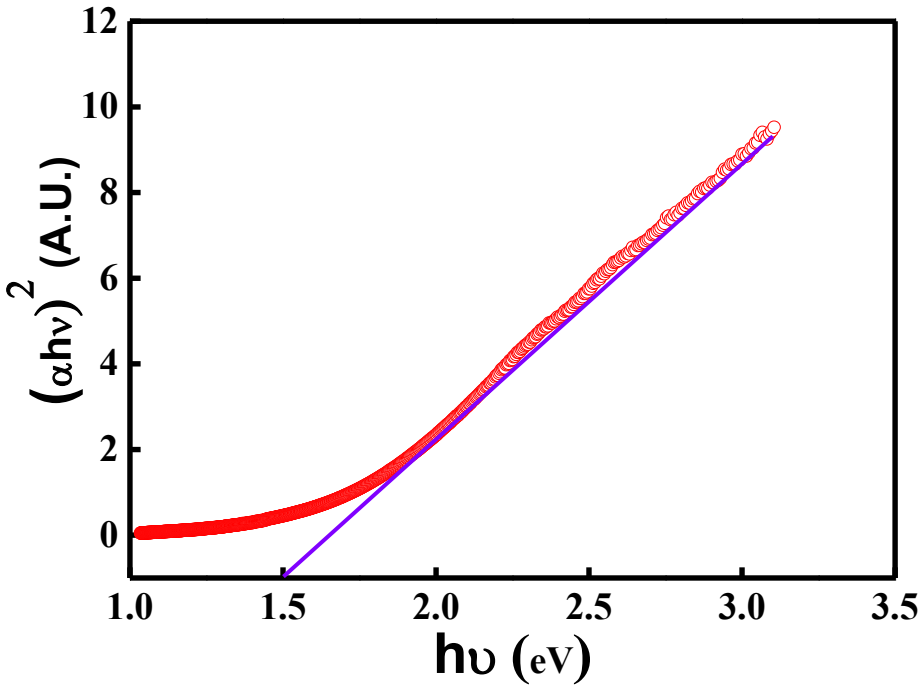

Figure 42: $(\alpha h\upsilon)^2$ vs photon energy ($h\upsilon$) plot.

PL spectroscopy was used to confirm the band gap of the CZTS thin film sample. Figure 43 shows the PL spectrum of CZTS thin film. The measurement was performed at room temperature with 532nm excitation wavelength. The result shows a symmetric and sharp peak at 1.5 eV. This peak is related to the transition of electrons from one band to another in CZTS thin film. Consequently, It is conformed that the band gap of the prepared CZTS thin film is 1.5 eV.

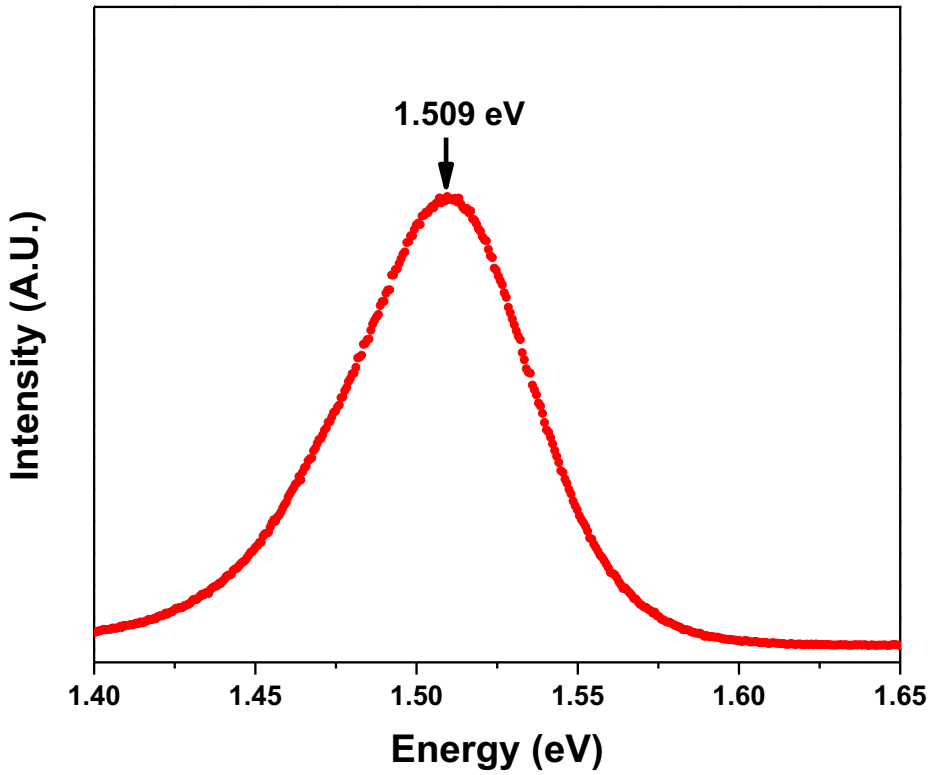

Figure 43: PL spectra of CZTS thin film deposited at -1.35 V and sulfurized using 35 mg of sulfur.

CHAPTER 5: CONCLUSION

In conclusion, CZTS thin films were deposited on FTO coated glass substrates using single step electrodeposition technique. An optimization process was done to identify the suitable deposition potential. A set of CZTS thin films were deposited using -1.10 V, -1.20 V, -1.25 V, -1.30 V, and -1.35 V (vs. Ag/AgCl) deposition potentials. After sulfurization, the films were characterized using different characterization techniques. The XRD and Raman analysis confirmed the formation of CZTS kesterite films in the samples. A dependence of the XRD intensity and FWHM of the (112) planes and crystallite size was observed. It was found that the sample deposited at -1.35 V exhibits the best crystalline quality and pure CZTS kesterite phase. It was observed that, as the deposition potential becomes more negative, the zinc atomic percentage is increasing, while the atomic percentage of copper is decreasing. The EDS and XPS measurements conducted on all samples proved that the sample deposited at -1.35 V has the best stoichiometry compared to other samples.

The effect of the sulfur amount in the sulfurization process on CZTS thin films was studied. For this purpose, A set of samples were deposited at -1.35 V and sulfurized using 5 mg, 15 mg, 25 mg, 35 mg, and 50 mg of sulfur powder. The XRD, Raman analysis, and EDS analysis proved the superiority of the stoichiometry and crystalline quality of the sample sulfurized with 35 mg sulfur to other samples. The CZTS film sulfurized using 50 mg sulfur exhibited an SnS secondary.

The UV-visible and PL measurements were used to identify the optical band gap and the absorption coefficient. From the UV-visible absorption spectrum, the optical band

gap of the film deposited using 35 mg of sulfur was estimated to be 1.51 eV and the absorption coefficient was determined to be 10^4 cm^{-1}. The PL spectrum peak at 1.51 eV corresponds to direct band transition in the film. These results confirm the suitability of these films to be utilized as absorber layers in thin film solar cell structures.

FUTURE WORK

The electrodeposited CZTS thin films at -1.35 V and sulfurized using 35 mg will be implemented as absorber layers in thin film solar cell structure as shown in figure 44.

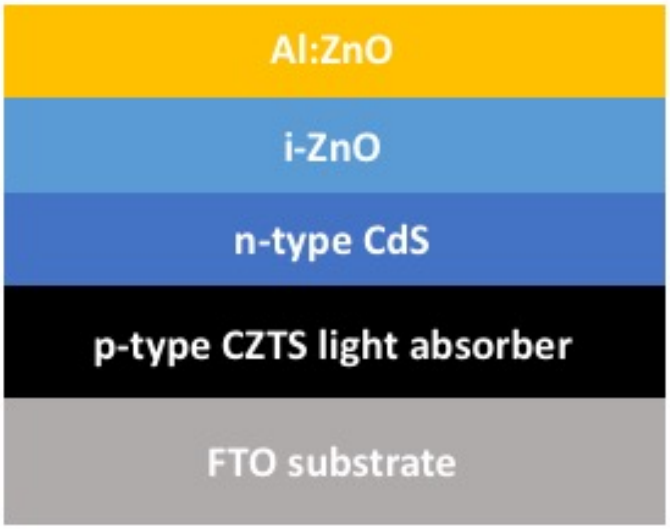

Figure 44: CZTS thin film solar cells structure.

REFERENCES

1. K.I. Jayawardena, L. J. R., C.A. Mills, M.J. Beliatis, N.A. Nismy, S.R.P. Silva,, Inorganics-in-Organics': recent developments and outlook for 4G polymer solar cells. *Nanoscale* **2013,** *5*, 8411-8427.

2. J.H. Zhao, A. H. W., M.A. Green, F. Ferrazza, 19.8% efficient "honeycomb" textured multicrystalline and 24.4% monocrystalline silicon solar cells. *Applied Physics Letters* **1998,** *73*, 1991-1993.

3. A. Shah, J. M., E. Vallat-Sauvain, N. Wyrsch, U. Kroll, C. Droz, U. Graf, Material and solar cell research in microcrystalline silicon. *Solar Energy Materials and Solar Cells* **2003,** *78*, 469-491.

4. I. Robel, V. S., M. Kuno, P.V. Kamat, Quantum dot solar cells. Harvesting light energy with CdSe nanocrystals molecularly linked to mesoscopic TiO2 films. *Journal of the American Chemical Society* **2006,** *128*, 2385-2393.

5. B. O'Regan, M. G., A low-cost, high-efficiency solar cell based on dye-sensitized colloidal TiO2 films. *nature:Scientific reports* **1991,** *353*, 737-740.

6. Li, L.; Wang, Y. Q.; Deng, X. L.; Nie, L. H.; Cui, Z. D.; Shi, C. W., Br-Doping CH3NH3PbI3-xBrx Thin Films for Efficient TiO2 Nanorod Array Perovskite Solar Cells. *J Nanosci Nanotechno* **2018,** *18* (7), 5095-5100.

7. A. Feltrin, A. F., Material considerations for terawatt level deployment of photovoltaics. *Renewable Energy* **2008,** *33*, 180-185.

8. Garcia, C.; Bollero, A.; Friedrich, E. J.; Leon, M.; Gutierrez, M. T.; de Abajo, J., Molybdenum-coated hybrid polyimide composites as back contact layers for flexible solar cells. *J Phys Chem Solids* **2013,** *74* (5), 702-707.

9. C. Malerba, F. B., C. L. Azanza Ricard, M. Valentini, R. Chierchia, M. Müller, A. Santoni, E. Esposito, P. Mangiapane, P. Scardi, A. Mittiga, J. , CZTS stoichiometry effects on the band gap energy,. *Alloys Compd.* **2014,** *582*.

10. Jackson, P.; Wuerz, R.; Hariskos, D.; Lotter, E.; Witte, W.; Powalla, M., Effects of heavy alkali elements in Cu(In,Ga)Se2solar cells with efficiencies up to 22.6%. *physica status solidi (RRL) - Rapid Research Letters* **2016,** *10* (8), 583-586.

11. Zhao, Y.; Burda, C., Development of plasmonic semiconductor nanomaterials with copper chalcogenides for a future with sustainable energy materials. *Energy Environ. Sci.* **2012,** *5* (2), 5564-5576.

12. Schäfer, W. N., *Mater. Res. Bull.* **1974,** *9*, 645–654.

13. Shin, B.; Zhu, Y.; Bojarczuk, N. A.; Jay Chey, S.; Guha, S., Control of an interfacial MoSe2 layer in Cu2ZnSnSe4 thin film solar cells: 8.9% power conversion efficiency with a TiN diffusion barrier. *Applied Physics Letters* **2012,** *101* (5).

14. Chen, S.; Gong, X. G.; Walsh, A.; Wei, S.-H., Crystal and electronic band structure of Cu2ZnSnX4 (X=S and Se) photovoltaic absorbers: First-principles insights. *Applied Physics Letters* **2009,** *94* (4).

15. Olekseyuka, I. D.; Gulayb, L. D.; Dydchaka, I. V.; Piskacha, L. V.; Parasyuka, O. V.; , O. V. M., Single crystal preparation and crystal structure of the Cu2Zn/Cd,Hg/SnSe4 compounds. *Journal of Alloys and Compounds* **2002,** *340*, 141-145.

16. I. Olekseyuk, I. D., L. Piskach, Phase equilibria in the Cu2S–ZnS–SnS2 system. *Journal of Alloys and Compounds* **2004,** *368*, 135-143.

17. S. Chen, A. W., X.G. Gong, S.H. Wei, Classification of Lattice Defects in the Kesterite Cu2ZnSnS4 and Cu2ZnSnSe4 Earth-Abundant Solar Cell Absorbers. *Advanced Materials* **2013,** *25*, 1522-1539.

18. T.K. Todorov, J. T., S. Bag, O. Gunawan, T. Gokmen, Y. Zhu, D.B. Mitzi, , , Beyond 11% efficiency: characteristics of state-of-the-art Cu2ZnSn (S, Se)4 solar cells. *Advanced Energy Materials,* **2013,** *3*, 34-38.

19. Shin, y.; Gunawan, O.; Zhu, Y.; Bojarczuk, N. A.; Chey, S. J.; Guha, S., Thin film solar cell with 8.4% power conversion efficiency using an earth-abundant Cu2ZnSnS4 absorber. *PROGRESS IN PHOTOVOLTAICS: RESEARCH & APPLICATIONS* **2011,** *21*, 72-76.

20. B. Shin, O. G., Thin film solar cell with 8.4% power conver- sion e ciency using an earth-abundant Cu2ZnSnS4 absorber. *Progress in Photovoltaics: Research and Applications* **2011**.

21. D.A.R. Barkhouse, O. G., T. Gokmen, T.K. Todorov, D.B. Mitzi, Device characteristics of a 10.1% hydrazine-processed Cu2ZnSn(Se, S)4 solar cell. *Progress in Photovoltaics: Research and Applications,* **2012,** *20*, 6-11.

22. Ahmed, S.; Reuter, K. B.; Gunawan, O.; Guo, L.; Romankiw, L. T.; Deligianni, H., A High Efficiency Electrodeposited Cu2ZnSnS4 Solar Cell. *Advanced Energy Materials* **2012,** *2* (2), 253-259.

23. Engman, J., Experimental study of Cu2ZnSn(Se,S)4 thin films for solar cell applications,. *Thesis, Uppsala university,USA* **2011**.

24. K.P. Musselman, L. S.-M., Nanostructured inorganic solar cells. *Green Chemistry* **2011,** *1*, 7-27.

25. Keiichiro Masuko, M. S., Taiki Hashiguchi, *Ieee J Photovolt* **2014**, 1433-1435.

26. Li, Y. G.; Du, D. X., Characterization of Amorphous Silicon Thin Films Deposited on Upilex-s Polyimide Substrates for Application in Flexible Solar Cells. *Adv Mater Res-Switz* **2010,** *87-88*, 416-+.

27. Aksu, S.; Lastella, S.; Kleiman-Shwarsctein, A.; Pinarbasi, M., Electrodeposition of Novel Precursor Structures for Efficient Copper Indium Gallium Selenide (CIGS) Films. *Ecs Transactions* **2011,** *35* (21), 33-38.

28. Chen, Y. F.; Tan, X. H.; Peng, S.; Xin, C.; Delahoy, A. E.; Chin, K. K.; Zhang, C. J., The Influence of Conduction Band Offset on CdTe Solar Cells. *J Electron Mater* **2018,** *47* (2), 1201-1207.

29. Jackson, P.; Hariskos, D.; Lotter, E.; Paetel, S.; Wuerz, R.; Menner, R.; Wischmann, W.; Powalla, M., New world record efficiency for Cu(In,Ga)Se2 thin-film solar cells beyond 20%. *Progress in Photovoltaics: Research and Applications* **2011,** *19* (7), 894-897.

30. XuanzhiWu, High-efficiency polycrystalline CdTe thin-film solar cells. *Sol Energy* **2004,** *77* (6), 803-814.

31. MichaelGrätzel, Dye-sensitized solar cells. *Journal of Photochemistry and Photobiology C: Photochemistry Reviews* **2003,** *4* (2), 145-153.

32. Lee, Y. L.; Lo, Y. S., Highly Efficient Quantum-Dot-Sensitized Solar Cell Based on Co-Sensitization of CdS/CdSe. *Adv Funct Mater* **2009,** *19* (4).

33. Seok, S. I.; Gratzel, M.; Park, N. G., Methodologies toward Highly Efficient Perovskite Solar Cells. *Small* **2018**.

34. Bag, S.; Gunawan, O.; Gokmen, T.; Zhu, Y.; Todorov, T. K.; Mitzi, D. B., Low band gap liquid-processed CZTSe solar cell with 10.1% efficiency. *Energy & Environmental Science* **2012,** *5* (5).

35. Wang, W.; Winkler, M. T.; Gunawan, O.; Gokmen, T.; Todorov, T. K.; Zhu, Y.; Mitzi, D. B., Device Characteristics of CZTSSe Thin-Film Solar Cells with 12.6% Efficiency. *Advanced Energy Materials* **2014,** *4* (7).

36. Homare, H., Noriyuki, S., Takuya, K., Hiroki, S., High Voltage Cu2ZnSnS4 Submodules by Hybrid Buffer Layer. . *IEEE Photovoltaic Specialists Conference* **2013**.

37. K. Ito; Nakazawa, T., Electrical and optical properties of stannite-type quaternary semiconductor thin films. *Japanese Journal of Applied Physics* **1988,** *27*, 2094-2097.

38. Wang, H., Progress in Thin Film Solar Cells Based onCu2ZnSnS4. *International Journal of Photoenergy* **2011,** *2011*, 1-10.

39. Song, X.; Ji, X.; Li, M.; Lin, W.; Luo, X.; Zhang, H., A Review on Development Prospect of CZTS Based Thin Film Solar Cells. *International Journal of Photoenergy* **2014,** *2014*, 1-11.

40. Hiroi, H.; Sakai, N.; Kato, T.; Sugimoto, H., High voltage Cu<inf>2</inf>ZnSnS<inf>4</inf> submodules by hybrid buffer layer. In *2013 IEEE 39th Photovoltaic Specialists Conference (PVSC)*, 2013; pp 0863-0866.

41. Kobayashi, T.; Jimbo, K.; Tsuchida, K.; Shinoda, S.; Oyanagi, T.; Katagiri, H., Investigation of Cu2ZnSnS4-Based Thin Film Solar Cells Using Abundant Materials. *Japanese Journal of Applied Physics* **2005,** *44* (1B), 783-787.

42. Balaji, G.; Balasundaraprabhu, R.; Prasanna, S.; Prabavathy, N.; McIlroy, D. N.; Kannan, M. D., Investigations of RF magnetron sputtered CZTS absorber layer thin films prepared using sulfur induced binary targets without sulfurization. *Opt Mater* **2018,** *75*, 56-60.

43. Liu, L. L.; Jiao, Y. X.; Gao, C.; Xu, H. J.; Zhao, W.; Dai, W. J.; Yu, W.; Li, X. W., Improving the performance of Cu2Zn(SnyGe1-y)(SxSe1-x)(4) solar cells by CdS:Zn buffer layers. *Journal of Alloys and Compounds* **2018,** *738*, 158-163.

44. Muhunthan, N.; Singh, O. P.; Singh, S.; Singh, V. N., Growth of CZTS Thin Films by Cosputtering of Metal Targets and Sulfurization in H2S. *International Journal of Photoenergy* **2013,** *2013*, 1-7.

45. Dalapati, G. K.; Zhuk, S.; Masudy-Panah, S.; Kushwaha, A.; Seng, H. L.; Chellappan, V.; Suresh, V.; Su, Z. H.; Batabyal, S. K.; Tan, C. C.; Guchhait, A.; Wong, L. H.; Wong, T. K. S.; Tripathy, S., Impact of molybdenum out diffusion and interface quality on the performance of sputter grown CZTS based solar cells. *Sci Rep-Uk* **2017,** *7*.

46. Moholkar, A. V.; Shinde, S. S.; Babar, A. R.; Sim, K.-U.; Lee, H. K.; Rajpure, K. Y.; Patil, P. S.; Bhosale, C. H.; Kim, J. H., Synthesis and characterization of Cu2ZnSnS4 thin films grown by PLD: Solar cells. *Journal of Alloys and Compounds* **2011,** *509* (27), 7439-7446.

47. Moholkar, A. V.; Shinde, S. S.; Agawane, G. L.; Jo, S. H.; Rajpure, K. Y.; Patil, P. S.; Bhosale, C. H.; Kim, J. H., Studies of compositional dependent CZTS thin film solar cells by pulsed laser deposition technique: An attempt to improve the efficiency. *Journal of Alloys and Compounds* **2012,** *544*, 145-151.

48. Li, Y.; Chen, J. F.; Ma, J. H.; Zhou, L. F., The optimization functions of ICP discharge in preparation of Cu-Zn-Sn precursors and CZTS films by co-evaporation. *J Semicond* **2016,** *37* (2).

49. Zhang, J.; Long, B.; Cheng, S. Y.; Zhang, W. B., Effects of Sulfurization Temperature on Properties of CZTS Films by Vacuum Evaporation and Sulfurization Method. *International Journal of Photoenergy* **2013**.

50. Li, Y.; Chen, J. F.; Ma, J. H., Properties of Cu2ZnSnS4 (CZTS) thin films prepared by plasma assisted co-evaporation. *J Mater Sci-Mater El* **2015,** *26* (9), 6546-6551.

51. Washio, T.; Shinji, T.; Tajima, S.; Fukano, T.; Motohiro, T.; Jimbo, K.; Katagiri, H., 6% Efficiency Cu2ZnSnS4-based thin film solar cells using oxide precursors by open atmosphere type CVD. *Journal of Materials Chemistry* **2012,** *22* (9).

52. Ansari, M. Z.; Khare, N., Structural and optical properties of CZTS thin films deposited by ultrasonically assisted chemical vapour deposition. *J Phys D Appl Phys* **2014,** *47* (18).

53. Htay, M. T.; Hashimoto, Y.; Momose, N.; Sasaki, K.; Ishiguchi, H.; Igarashi, S.; Sakurai, K.; Ito, K., A Cadmium-Free Cu2ZnSnS4/ZnO Hetrojunction Solar Cell Prepared by Practicable Processes. *Japanese Journal of Applied Physics* **2011,** *50*.

54. Chtouki, T.; Soumahoro, L.; Kulyk, B.; Bougharraf, H.; Erguig, H.; Ammous, K.; Sahraoui, B., Comparative Study on the Structural, Morphological, Linear and Nonlinear Optical Properties of CZTS Thin Films Prepared by Spin-Coating and Spray Pyrolysis. *Mater Today-Proc* **2017,** *4* (4), 5146-5153.

55. Ramirez, E.; Ramirez, A. A.; Hurtado, M. F.; Gordillo, G., Microstructural and optical characterization of CZTS thin films deposited in one step by spray pyrolysis. *2015 Ieee 42nd Photovoltaic Specialist Conference (Pvsc)* **2015**.

56. Exarhos, S.; Bozhilov, K. N.; Mangolini, L., Spray pyrolysis of CZTS nanoplatelets. *Chem Commun* **2014,** *50* (77), 11366-11369.

57. Aono, M.; Yoshitake, K.; Miyazaki, H., XPS depth profile study of CZTS thin films prepared by spray pyrolysis. *Physica Status Solidi C: Current Topics in Solid State Physics, Vol 10, No 7-8* **2013,** *10* (7-8), 1058-1061.

58. Prabhakar, T.; Nagaraju, J., Ultrasonic Spray Pyrolysis of Czts Solar Cell Absorber Layers and Characterization Studies. *35th Ieee Photovoltaic Specialists Conference* **2010**, 1964-1969.

59. Su, Z.; Sun, K.; Han, Z.; Cui, H.; Liu, F.; Lai, Y.; Li, J.; Hao, X.; Liu, Y.; Green, M. A., Fabrication of Cu2ZnSnS4solar cells with 5.1% efficiency via thermal decomposition and reaction using a non-toxic sol–gel route. *J. Mater. Chem. A* **2014,** *2* (2), 500-509.

60. Swami, S. K.; Kumar, A.; Dutta, V., Deposition of Kesterite Cu2ZnSnS4 (CZTS) Thin Films by Spin Coating Technique for Solar Cell Application. *Pv Asia Pacific Conference 2012* **2013,** *33*, 198-202.

61. Jiang, F.; Ikeda, S.; Tang, Z.; Minemoto, T.; Septina, W.; Harada, T.; Matsumura, M., Impact of alloying duration of an electrodeposited Cu/Sn/Zn metallic stack on properties of Cu2ZnSnS4absorbers for thin-film solar cells. *Progress in Photovoltaics: Research and Applications* **2015,** *23* (12), 1884-1895.

62. Mangan, T. C.; McCandless, B. E.; Dobson, K. D.; Birkmire, R. W., Thermochemical and kinetic aspects of Cu2ZnSn(S,Se)4 thin film growth by reacting Cu-Zn-Sn precursors in H2S and H2Se. *Journal of Applied Physics* **2015,** *118* (6).

63. Chen, H.; Ye, Q.; He, X.; Ding, J.; Zhang, Y.; Han, J.; Liu, J.; Liao, C.; Mei, J.; Lau, W., Electrodeposited CZTS solar cells from Reline electrolyte. *Green Chem.* **2014,** *16* (8), 3841-3845.

64. Tao, J.; Zhang, K.; Zhang, C.; Chen, L.; Cao, H.; Liu, J.; Jiang, J.; Sun, L.; Yang, P.; Chu, J., A sputtered CdS buffer layer for co-electrodeposited Cu2ZnSnS4 solar cells with 6.6% efficiency. *Chem Commun (Camb)* **2015,** *51* (51), 10337-40.

65. J.J. Scragg, P. J. D., L.M. Peter, G. Zoppi,I. Forbes, New routes to sustainable photovoltaics: evaluation of Cu2ZnSnS4as an alternative absorber material. *Phys. Status Solidi B* **2008,** *245*, 1772.

66. J.J. Scragg, D. M. B., P.J. Dale, A 3.2% efficient Kesterite device from electrodeposited stacked elemental layers. *Electroanal. Chem.* **2010,** *646*, 52.

67. J.J. Scragg, P. J. D. a. L. M. P., Synthesis and characterization of Cu2ZnSnS4 absorber layers by an electrodeposition-annealing route. *Thin Solid Films* **2008,** *517*, 2481-2484.

68. F. Jiang, S. I., T. Harada, M. Matsumura, Pure sulfide Cu2ZnSnS4 thin film solar cells fabricated by preheating an electrodeposited metallic stack. *Advanced Energy Materials* **2014,** *4*.

69. F. Jiang, S. I., Z. Tang, T. Minemoto, W. Septina, T. Harada, M. Matsumura, Impact of alloying duration of an electrodeposited Cu/Sn/Zn metallic stack on properties of Cu2ZnSnS4 absorbers for thin- film solar cells. *rogress in Photovoltaics: Research and Applications* **2015**.

70. Guo, L.; Zhu, Y.; Gunawan, O.; Gokmen, T.; Deline, V. R.; Ahmed, S.; Romankiw, L. T.; Deligianni, H., Electrodeposited Cu2ZnSnSe4thin film solar cell with 7% power conversion efficiency. *Progress in Photovoltaics: Research and Applications* **2014,** *22* (1), 58-68.

71. Y. Lin, S. I., W. Septina, Y. Kawasaki, T. Harada, M. Matsumura, Mechanistic aspects of preheating effects of electrodeposited metallic precursors on structural and

photovoltaic properties of Cu2ZnSnS4 thin films,. *Solar Energy Materials and Solar Cells* **2014,** *120*, 218-225.

72. X. He, H. S., J. Pi, C. Zhang, Y. Hao, Synthesis of Cu2ZnSnS4 films from sequentially electrodeposited Cu–Sn–Zn precursors and their structural and optical properties. *Journal of Materials Science: Materials in Electronics* **2013,** *24*, 4578-4584.

73. T. Yuan, Y. L., M. Jia, Y. Lai, J. Li, F. Liu, Y. Liu, Fabrication of Cu2ZnSnS4 thin film solar cell bu sulfrization of electrodeposited stacked binary Cu-Zn and Cu-Sn alloy layers. *Materials Letters* **2015,** *155*, 44-47.

74. Ennaoui, A.; Lux-Steiner, M.; Weber, A.; Abou-Ras, D.; Kötschau, I.; Schock, H. W.; Schurr, R.; Hölzing, A.; Jost, S.; Hock, R.; Voß, T.; Schulze, J.; Kirbs, A., Cu2ZnSnS4 thin film solar cells from electroplated precursors: Novel low-cost perspective. *Thin Solid Films* **2009,** *517* (7), 2511-2514.

75. Araki, H.; Kubo, Y.; Jimbo, K.; Maw, W. S.; Katagiri, H.; Yamazaki, M.; Oishi, K.; Takeuchi, A., Preparation of Cu2ZnSnS4 thin films by sulfurization of co-electroplated Cu- Zn-Sn precursors. *Phys. Status Solidi C* **2009,** *6*, 1266.

76. Y. Li, T. Y., L. Jiang, Z. Su and F. Liu, J. , Alloys Compd. **2014,** *610*, 331.

77. E. Rakhshani, A., One-Step Electrodeposition of CuZnSn Metal Alloy Precursor Film Followed by the Synthesis of Cu2ZnSnS4 and Cu2ZnSnSe4 Light Absorber Films and Heterojunction Devices. *International Journal of Electrochemical Science* **2017**, 7786-7794.

78. Pawar, S. M.; Pawar, B. S.; Moholkar, A. V.; Choi, D. S.; Yun, J. H.; Moon, J. H.; Kolekar, S. S.; Kim, J. H., Single step electrosynthesis of Cu2ZnSnS4 (CZTS) thin films for solar cell application. *Electrochimica Acta* **2010,** *55* (12), 4057-4061.

79. J. Ge, J. C., J. Jiang, Y. Yan, P. Yang, Characteristics of In-substituted CZTS thin film and bifacial solar cell. *ACS Applied Materials & Interfaces* **2014,** *6*, 21118-21130.

80. Lee, S. G.; Kim, J.; Woo, H. S.; Jo, Y.; Inamdar, A. I.; Pawar, S. M.; Kim, H. S.; Jung, W.; Im, H. S., Structural, morphological, compositional, and optical properties of single step electrodeposited Cu2ZnSnS4 (CZTS) thin films for solar cell application. *Current Applied Physics* **2014,** *14* (3), 254-258.

81. Mg, L.; Gr, B., Electrochemical Synthesis and Characterization of Cu2ZnSnS4 Thin Films. *Journal of Material Science & Engineering* **2016,** *5* (4).

82. Tang, A.; Li, Z.; Wang, F.; Dou, M.; Pan, Y.; Guan, J., One step electrodeposition of Cu 2 ZnSnS 4 thin films in a novel bath with sulfurization free annealing. *Applied Surface Science* **2017,** *402*, 70-77.

83. Jiahua Tao, J. H., Kezhi Zhang, Junfeng Liu, Yuchen Dong, Lin Sun n, Pingxiong Yang, Junhao Chu, Effect of deposition potential on the properties of Cu2ZnSnS4 films for solar cell applications. *Materials Letters* **2014,** *135*, 8-10.

84. M. Beres, J. S., K.M. Yu , S.S. Mao Growth behavior of co-electrodeposited CZTS precursor thin films from acidic baths containing tartaric acid. *Materials Chemistry and Physics* **2017,** *204*, 83-94.

85. Ananthoju, B.; Sonia, F. J.; Kushwaha, A.; Bahadur, D.; Medhekar, N. V.; Aslam, M., Improved structural and optical properties of Cu2ZnSnS4 thin films via optimized potential in single bath electrodeposition. *Electrochimica Acta* **2014,** *137*, 154-163.

86. Cao, M.; Li, L.; Zhang, B. L.; Huang, J.; Wang, L. J.; Shen, Y.; Sun, Y.; Jiang, J. C.; Hu, G. J., One-step deposition of Cu2ZnSnS4 thin films for solar cells. *Solar Energy Materials and Solar Cells* **2013,** *117*, 81-86.

87. Zhang, H.; Cheng, S.; Yu, J.; Lai, Y.; Zhou, H.; Jia, H., Effects of pH Value in the Electrolyte on the Properties of Cu2ZnSnS4Thin Film Fabricated by Single Step Co-Electrodeposition. *ECS Journal of Solid State Science and Technology* **2016,** *5* (9), P521-P525.

88. Agasti, A.; Mallick, S.; Bhargava, P., Electrolyte pH dependent controlled growth of co-electrodeposited CZT films for application in CZTS based thin film solar cells. *Journal of Materials Science: Materials in Electronics* **2017,** *29* (5), 4065-4074.

89. R. SANI, R. M., S. N. VICTORIA, ONE STEP ELECTROCHEMICAL DEPOSITION OF CZTS FOR SOLAR CELL APPLICATIONS
. *Chalcogenide Letters* **2017,** *14*, 165 - 170.

90. Pawar, B. S.; Pawar, S. M.; Shin, S. W.; Choi, D. S.; Park, C. J.; Kolekar, S. S.; Kim, J. H., Effect of complexing agent on the properties of electrochemically deposited Cu2ZnSnS4 (CZTS) thin films. *Applied Surface Science* **2010,** *257* (5), 1786-1791.

91. Jeon, M.; Tanaka, Y.; Shimizu, T.; Shingubara, S., Formation and characterization of single-step electrodeposited Cu2ZnSnS4 thin films: Effect of complexing agent volume. *Energy Procedia* **2011,** *10*, 255-260.

92. Mkawi, E. M.; Ibrahim, K.; Ali, M. K. M.; Farrukh, M. A.; Mohamed, A. S.; Allam, N. K., Effect of complexing agents on the electrodeposition of Cu–Zn–Sn metal precursors and corresponding Cu2ZnSnS4-based solar cells. *Journal of Electroanalytical Chemistry* **2014,** *735*, 129-135.

93. Araki, H.; Kubo, Y.; Mikaduki, A.; Jimbo, K.; Maw, W. S.; Katagiri, H.; Yamazaki, M.; Oishi, K.; Takeuchi, A., Preparation of Cu2ZnSnS4 thin films by sulfurizing electroplated precursors. *Solar Energy Materials and Solar Cells* **2009,** *93* (6-7), 996-999.

94. Mkawi, E. M.; Ibrahim, K.; Ali, M. K. M.; Farrukh, M. A.; Mohamed, A. S., Dependence of the properties of copper zinc tin sulfide thin films prepared by electrochemical deposition on sulfurization temperature. *Journal of Materials Science: Materials in Electronics* **2013,** *25* (2), 857-863.

95. Mkawi, E. M.; Ibrahim, K.; Ali, M. K. M.; Saron, K. M. A.; Farrukh, M. A.; Allam, N. K., Influence of substrate temperature on the properties of electrodeposited kesterite Cu2ZnSnS4 (CZTS) thin films for photovoltaic applications. *Journal of Materials Science: Materials in Electronics* **2014,** *26* (1), 222-228.

96. He, H. G. H. S. C. G. X., Sulfurization time effects on the growth of Cu2ZnSnS4 thin films by solution method. *Mater Sci: Mater Electron* **2013,** *24*, 2667-2671.

97. Ali Aldalbahi, E. M. M., K. Ibrahim & M. A. Farrukh, Effect of sulfurization time on the properties of copper zinc tin sul de thin lms grown by electrochemical deposition. *nature:Scientific reports* **2016,** *6*, 32431.

98. telter, M. B., H. , Process Optimization in Copper Electrorefining". . *Advanced Engineering Materials.* **2004,** *6* (7), 558.

99. Bard, A. J. L. R., *Electrochemical Methods: Fundamentals and Applications*. Wiley: 2000.

100. Heinze, J. C. V.-E. S. N. A. M. A. C. I. E. i. E., Cyclic Voltammetry-"Electrochemical Spectroscopy. *New Analytical Methods* **1984,** *23* (11), 831–847.

101. Nicholson, R. S. I., "Theory of Stationary Electrode Polarography. Single Scan and Cyclic Methods Applied to Reversible, Irreversible, and Kinetic Systems". *Anal Chem* **1964,** *36* (4), 706–723.

102. Theivasanthi, T.; Alagar, M., X-Ray Diffraction Studies of Copper Nanopowder.

103. Bruker Corporation.

104. VD Mote, Y. P., BN Dole, Journal of Theoretical and Applied Physics. **2012,** *6*, 2251-7235.

105. K. Venkateswarlu, A. C., N.Rameshbabu, *Physica B* **2010,** *405*, 4256-4261.

106. L. Kissel, R. H. P., A 46 (1990) 170., *ActaCrystallographica A* **1990,** *170*.

107. Toney, J., *Characterization of Materials*. E. N. Kaufmann (Ed.): 2002.

108. Schroeder; K, D., *Semiconductor Material and Device Characterization*. 2nd edition ed.; Wiley-Interscience: 1998.

109. FEI (part of Thermo Fisher Scientific).

110. Ohring, M., *Materials Science of Thin Films*. 2nd edition ed.; Elsevier Inc: 2002.

111. Shindo D., O. T., *Energy Dispersive X-ray Spectroscopy. In: Analytical Electron Microscopy for Materials Science.* Springer: Tokyo, 2002.

112. P.J., P., *Energy dispersive x-ray spectrometry. In: A Handbook of Silicate Rock Analysis.* Springer: Dordrecht, 1987.

113. Dongwoo Optron Co.

114. Tissue, B. M., Ultraviolet and Visible Absorption Spectroscopy. *wiley* **2002**.

115. Wang, Z.; Tao, J.; Xiao, W.; Xu, T.; Zhang, X.; Hu, D.; Ma, Z., Influence of deposition potential on Cu 2 ZnSnS 4 thin–film solar cells co–electrodeposited on fluorine–doped tin oxide substrates. *Journal of Alloys and Compounds* **2017,** *701*, 465-473.

116. J. Tao, L. C., H. Cao, C. Zhang, J. Liu, Y. Zhang, L. Huang, J. Jiang, P. Yang, J. Chu, , J. A,, Co–electrodeposited Cu2ZnSnS4 thin–film solar cells with over 7% efficiency fabricated via fine–
tuning of the Zn content in absorber layers. *J. Mater. Chem. A* **2016,** *4*, 3798–3805.

117. W. Dang, X. R., W. Zi, L. Jia, S. Liu, , Composition controlled preparation of Cu–Zn–Sn precursor films for Cu2ZnSnS4 solar cells using pulsed electrodeposition. *J. Alloys Compd.* **2015,** *650*, 1-7.

118. Septina, W.; Ikeda, S.; Kyoraiseki, A.; Harada, T.; Matsumura, M., Single-step electrodeposition of a microcrystalline Cu2ZnSnSe4 thin film with a kesterite structure. *Electrochimica Acta* **2013,** *88*, 436-442.

119. Scragg, J. J.; Berg, D. M.; Dale, P. J., A 3.2% efficient Kesterite device from electrodeposited stacked elemental layers. *Journal of Electroanalytical Chemistry* **2010,** *646* (1-2), 52-59.

120. Tao, J. H.; Chen, L. L.; Cao, H. Y.; Zhang, C. J.; Liu, J. F.; Zhang, Y. B.; Huang, L.; Jiang, J. C.; Yang, P. X.; Chu, J. H., Co-electrodeposited Cu2ZnSnS4 thin-film solar cells with over 7% efficiency fabricated via fine-tuning of the Zn content in absorber layers. *J Mater Chem A* **2016,** *4* (10), 3798-3805.

121. Tao, J. H.; Liu, J. F.; He, J.; Zhang, K. Z.; Jiang, J. C.; Sun, L.; Yang, P. X.; Chu, J. H., Synthesis and characterization of Cu2ZnSnS4 thin films by the sulfurization of co-electrodeposited Cu-Zn-Sn-S precursor layers for solar cell applications. *Rsc Adv* **2014,** *4* (46), 23977-23984.

122. Tao, J. H.; He, J.; Zhang, K. Z.; Liu, J. F.; Dong, Y. C.; Sun, L.; Yang, P. X.; Chu, J. H., Effect of deposition potential on the properties of Cu2ZnSnS4 films for solar cell applications. *Materials Letters* **2014,** *135*, 8-10.

123. Ge, J.; Jiang, J. C.; Yang, P. X.; Peng, C.; Huang, Z. P.; Zuo, S. H.; Yang, L. H.; Chu, J. H., A 5.5% efficient co-electrodeposited ZnO/CdS/Cu2ZnSnS4/Mo thin film solar cell. *Solar Energy Materials and Solar Cells* **2014,** *125*, 20-26.

124. Tiong, V. T. Z., Y.; Bell, J. M.; Wang, *H. CrystEngComm* **2014**.

125. Riha, S. C. P., B. A.; Prieto, A. L. J. Am. , *Chem. Soc.* **2009,** *131*, 12054–12055.

126. Wang, D.; Zhao, W.; Zhang, Y.; Liu, S., Path towards high-efficient kesterite solar cells. *Journal of Energy Chemistry* **2017**.

127. Ganchev, M.; Vitanov, P.; Sendova-Vassileva, M.; Popkirov, G.; Dikov, H., Properties of SnS thin films grown by physical vapour deposition. *Journal of Physics: Conference Series* **2016,** *682*.

128. H. Cao, H. D., L. Chen, J. Tao, X. Meng, J. Liu, F. Yue, L. Sun, P. Yang, J. Chu, A, J. , ntimony–
induced grain growth and properties modification of Cu(In, Al)Se2 thin films fabricated by
selenization of sputtered stacked precursors. *Alloys Compd.* **2016,** *689*, 21–29.
129. X. Meng, H. D., J. Tao, H. Cao, X. Li, L Sun, P. Yang, J Chu,, Heating rate tuning in structure, morphology and electricity properties of Cu2FeSnS4 thin films prepared by sulfurization of
metallic precursors. . *Alloys Compd.* **2016,** *680* 446–451.